# A Variational Method for Analyzing Vortex Flows in Radar-Scanned Tornadic Mesocyclones. Part I: Formulations and Theoretical Considerations

QIN XU[a]

[a] *NOAA/OAR/National Severe Storms Laboratory, Norman, Oklahoma*

(Manuscript received 24 May 2020, in final form 5 November 2020)

ABSTRACT: A variational method is formulated with theoretical considerations for analyzing vortex flows in Doppler radar–scanned tornadic mesocyclones. The method has the following features. (i) The vortex center axis (estimated as a continuous function of time and height in the four-dimensional space) is used as the vertical coordinate, so the coordinate system used for the analysis is slantwise curvilinear and nonorthogonal in general. (ii) The vortex flow (VF), defined by the three-dimensional vector wind minus the horizontal moving velocity of vortex center axis, is expressed in terms of the covariant basis vectors (tangent to the coordinate curves), so its axisymmetric part can be properly defined in that slantwise-curvilinear coordinate system. (iii) To satisfy the mass continuity automatically, the axisymmetric part is expressed by the scalar fields of azimuthally averaged tangential velocity and cylindrical streamfunction and the remaining asymmetric part is expressed by the scalar fields of streamfunction and vertically integrated velocity potential. (iv) VF-dependent covariance functions are formulated for these scalar variables and then deconvoluted to construct the square root of background error covariance matrix analytically with the latter used to transform the control vector to precondition the cost function. (v) The deconvoluted covariance functions and their transformed control variables satisfy two required boundary conditions (i.e., zero vertical velocity at the lower rigid boundary and zero cross-axis velocity along the vortex center axis), so the analyzed VF satisfies not only the mass continuity but also the two boundary conditions automatically.

KEYWORDS: Radars/Radar observations; Variational analysis; Data assimilation; Vertical coordinates

## 1. Introduction

Increasing lead times for tornado, severe thunderstorm, and flash flood warnings to reduce loss of life, injury, and economic costs of high-impact weather is absolutely necessary and critical for a Weather Ready Nation—a key mission goal in the research strategic plan of the National Oceanic and Atmospheric Administration (NOAA 2014). Toward this goal, a warn-on-forecast (WoF) system was envisioned and developed (Stensrud et al. 2009, 2013; Wheatley et al. 2015) as a probabilistic convective-scale ensemble analysis and forecast system that assimilates in-storm observations into a high-resolution convection-resolving model ensemble. However, since the pure-ensemble WoF system is not always robust enough for optimally reducing initial condition errors in all cases so far tested (Wheatley et al. 2015; Jones et al. 2016; Skinner et al. 2018), a three-dimensional ensemble–variational data assimilation algorithm was developed and tested (Gao and Stensrud 2014; Wang et al. 2019) aiming to improve the robustness of the WoF system. Beyond these efforts and progresses, analyzing three-dimensional (3D) vortex winds in radar-observed tornadic mesocyclones remains extremely difficult but critical for tornadic-storm data assimilation and forecasts (Snook et al. 2019).

Accurately analyzing the 3D vortex wind in a radar-observed tornadic mesocyclone requires the following two conditions be satisfied in the first place—A: The vortex center location should be estimated as a function of height and time accurately enough (with the estimated location error smaller than the radius of the true vortex core, that is, the radius of the maximum tangential velocity of the true vortex flow); and B: The background error covariance should be formulated with vortex-flow dependencies in and around the vortex core. These two conditions are neither satisfied by the current WoF system nor considered by the recent tornado-resolving ensemble analyses (Snook et al. 2016, 2019). On the other hand, as will be shown in this paper, a variational method can be formulated to satisfy the above two conditions, although the previously developed variational methods for analyzing storm winds from radar observations (Gao et al. 2013; Xu et al. 2010, 2015a) have an intrinsic limitation in analyzing vortex winds due to the absence of vortex-flow dependence in their background error covariance formulations.

To overcome the aforementioned intrinsic limitation, vortex-flow-dependent background error covariance functions were formulated in the two-dimensional (2D) variational method (2DVar) developed recently for analyzing horizontal vortex winds at low elevations in radar-scanned tornadic mesocyclones (Xu et al. 2015b). This 2DVar method can be extended to analyze vortex winds in 3D or 4D space. For such an extension, the vortex center axis must be estimated first as a continuous function of height and time in the 4D space to satisfy the aforementioned condition A, and a three-step method was developed to achieve this (Xu et al. 2017). Using the estimated vortex center axis as the vertical coordinate, the local Cartesian coordinate system can be transformed into a slantwise moving coordinate system cocentered with the estimated vortex center axis in the 4D space, and this slantwise moving coordinate system will be used in this paper to formulate the aforementioned variational method for analyzing 3D vortex winds in radar-scanned tornadic mesocyclones.

It has long been recognized that using a moving coordinate system, either explicitly or implicitly, can reduce the advection-caused errors in analyzing radar-observed moving storm systems, and the involved techniques and related merits have been studied

*Corresponding author*: Dr. Qin Xu, qin.xu@noaa.gov

DOI: 10.1175/JAS-D-20-0158.1

by many investigators (Gal-Chen 1982: Chong et al. 1983; Yang and Xu 1996; Zhang and Gal-Chen 1996; Caillault and Lemaitre 1999; Liou 1999, 2002; Liou et al. 2018; Liu et al. 2004; Shapiro et al. 2010, 2015). However, unlike the moving rigid coordinate systems considered in the previous studies, the moving coordinate system used in this paper is slantwise curvilinear and time varying in general. In this coordinate system, as will be seen in this paper, the vortex flow (VF), defined by the 3D vector wind minus the horizontal moving velocity of vortex center axis, should be expressed in terms of the covariant basis vectors (tangent to the coordinate curves) and then properly partitioned into an axisymmetric part and a remaining asymmetric part, so suitable momentum control variables can be defined for each part to satisfy the mass continuity with their background error covariance functions formulated in VF-dependent forms to satisfy not only the aforementioned condition B but also the required boundary conditions (see the end of section 2c). With the partitioned formulations, the axisymmetric part of VF can be analyzed, either separately in the first step or jointly with the asymmetric part in a single step. The partitioned formulations will be derived separately for each part and the method will be presented in two steps in this paper.

The paper is organized as follows. The coordinate transformation and related vortex flow partition are derived in section 2. The formulations for analyzing the axisymmetric part and the remaining asymmetric part of VF are presented in sections 3 and 4, respectively, where VF-dependent covariance functions are formulated and deconvoluted to construct the square root of background error covariance matrix analytically. Conclusions follow in section 5.

## 2. Coordinate transformation, VF partition, and background error partition

### a. Coordinate transformation

To formulate the background wind error covariance functions with desirable VF dependences in a generally slantwise moving cylindrical coordinate system cocentered with the vortex at each vertical level, we need to transform the local Cartesian coordinate system $(x, y, z, t)$ first into the following moving coordinate system:

$$(x', y', z', t') = (x - x_c, y - y_c, z, t), \tag{2.1a}$$

where $(x_c, y_c)$ is the vortex center location estimated as a continuous function of $(z, t)$ in the 4D space by the method of Xu et al. (2017). This transformation ensures that the origin of $(x', y')$ is cocentered and moves with $(x_c, y_c)$ on each vertical level (see Fig. 1a). The space and time differential operators are transformed by

$$(\nabla, \partial_z, \partial_t) = (\nabla', \partial_{z'} - \mathbf{x}_{cz} \cdot \nabla', \partial_{t'} - \mathbf{u}_c \cdot \nabla'), \tag{2.1b}$$

where $\nabla \equiv (\partial_x, \partial_y)^{\mathrm{T}}$, $\nabla' \equiv (\partial_{x'}, \partial_{y'})^{\mathrm{T}}$, $\mathbf{x}_c \equiv x_c\mathbf{i} + y_c\mathbf{j}$, $\mathbf{x}_{cz} \equiv \partial_z\mathbf{x}_c = \partial_z x_c\mathbf{i} + \partial_z y_c\mathbf{j} \equiv x_{cz}\mathbf{i} + y_{cz}\mathbf{j}$, $\mathbf{u}_c \equiv \partial_t\mathbf{x}_c = \partial_t x_c\mathbf{i} + \partial_t y_c\mathbf{j} \equiv u_c\mathbf{i} + v_c\mathbf{j}$ is the horizontal moving velocity of the vortex center axis as a function of height, and $(\mathbf{i}, \mathbf{j}, \mathbf{k})$ denote the unit vectors in $(x, y, z)$ directions. In $(x, y, z, t)$, the total wind is denoted by $(u, v, w)$,

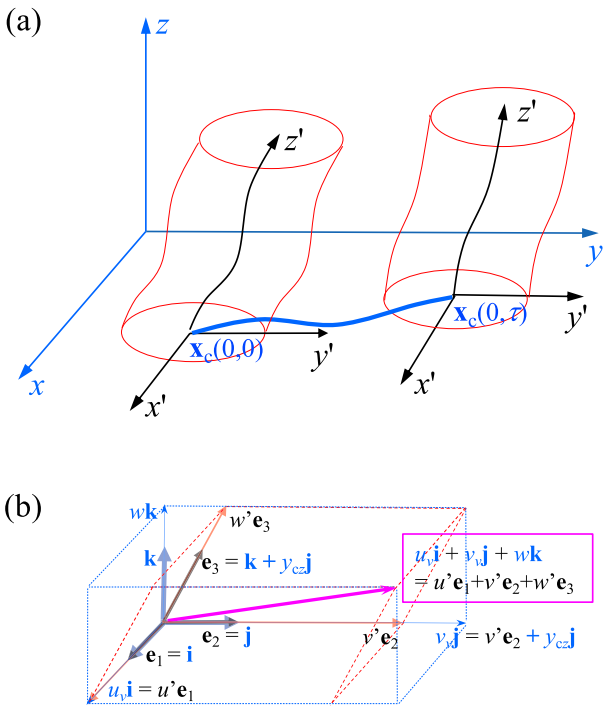


FIG. 1. (a) Vortex-following moving coordinate system $(x', y', z')$ plotted in black at $t' = t = 0$ and $t' = t = \tau$ in the local Cartesian coordinate system $(x, y, z)$ plotted in blue, where the thick blue curve shows the trajectory of the vortex center $\mathbf{x}_c(z, t)$ at $z = 0$ from $t = 0$ to $t = \tau$, and the two red slantwise curved cylinders show the vortex cores at $t = 0$ and $t = \tau$. (b) Covariant basis vectors $(\mathbf{e}_1, \mathbf{e}_2, \mathbf{e}_3)$ plotted by thick black arrows at a given point in $(x', y', z')$ and their relationships with the unit vectors $(\mathbf{i}, \mathbf{j}, \mathbf{k})$ plotted by thick blue arrows in $(x, y, z)$ directions, where the general relationship of $\mathbf{e}_3 = \mathbf{k} + \mathbf{x}_{cz}$ is simplified to $\mathbf{e}_3 = \mathbf{k} + y_{cz}\mathbf{j}$ by setting $\mathbf{x}_{cz} = y_{cz}\mathbf{j}$ with $x_{cz} = 0$ and thus is shown clearly in $(y, z)$ vertical plan. The thick purple arrow in (b) plots a 3D velocity vector of VF with its two equivalent expressions $u_v\mathbf{i} + v_u\mathbf{j} + w\mathbf{k} = u'\mathbf{e}_1 + v'\mathbf{e}_2 + w'\mathbf{e}_3$ written in the purple box, while the three component vectors of $u_v\mathbf{i} + v_u\mathbf{j} + w\mathbf{k}$ (or $u'\mathbf{e}_1 + v'\mathbf{e}_2 + w'\mathbf{e}_3$) are plotted by the thin blue (or red) arrows and labeled by blue (or black) letters.

and its vortex part, VF, is defined and denoted by $(u_v, v_v, w) \equiv (u–u_c, v–v_c, w)$. This vortex part can be also represented in $(x', y', z')$ in terms of its three contravariant components, defined and denoted by $(u', v', w') \equiv d_t(x', y', z')$, where $d_t \equiv \partial_t + \mathbf{u} \cdot \nabla + w\partial_z$ is the Lagrangian time derivative in $(x, y, z, t)$ where $\mathbf{u} = u\mathbf{i} + v\mathbf{j}$. The three covariant basis vectors for $(u', v', w')$ in $(x', y', z')$ are defined by $\mathbf{e}_1 \equiv \partial_{x'}(x\mathbf{i} + y\mathbf{j} + z\mathbf{k}) = \mathbf{i}$, $\mathbf{e}_2 \equiv \partial_{y'}(x\mathbf{i} + y\mathbf{j} + z\mathbf{k}) = \mathbf{j}$ and $\mathbf{e}_3 \equiv \partial_{z'}(x\mathbf{i} + y\mathbf{j} + z\mathbf{k}) = \mathbf{x}_{cz} + \mathbf{k}$, respectively (see Fig. 1b). Note that $\mathbf{e}_3 \cdot (\mathbf{i}, \mathbf{j}, \mathbf{k}) = (\partial_z x_c, \partial_z y_c, 1)$, so $\mathbf{e}_3$ is tangent to the $z'$-coordinate curve. Using the above introduced notations, the VF is represented by $u_v\mathbf{i} + v_u\mathbf{j} + w\mathbf{k}$ in $(x, y, z)$ and by $u'\mathbf{e}_1 + v'\mathbf{e}_2 + w'\mathbf{e}_3$ in $(x', y', z')$. The equivalence of these two representations (see Fig. 1b) leads to $(\mathbf{u}', w') = (\mathbf{u}_v–w\mathbf{x}_{cz}, w)$ or

$$(\mathbf{u}_v, w) = \left(\mathbf{u}' + w'\mathbf{x}_{cz}, w'\right), \tag{2.2}$$

where $\mathbf{u}' \equiv u'\mathbf{e}_1 + v'\mathbf{e}_2 = u'\mathbf{i} + v'\mathbf{j}$ and $\mathbf{u}_v \equiv u_v\mathbf{i} + v_u\mathbf{j}$.

The relationship derived in (2.2) can be also verified directly by substituting (2.1a) and (2.1b) into the definition of $(u', v', w') \equiv d_t(x', y', z')$, and this relationship can be written into a matrix form of $(u_v, v_v, w)^{\mathrm{T}} = \mathbf{J}(u', v', w')^{\mathrm{T}}$, where $\mathbf{J} = (\mathbf{e}_1, \mathbf{e}_2, \mathbf{e}_3)$ is a $3 \times 3$ matrix with its three columns given by the three covariant basis vectors defined above, and $(\ )^{\mathrm{T}}$ denotes the transpose of $(\ )$. Note that $\mathbf{J}$ is just the Jacobian matrix of the transformation from $(x', y', z')$ to $(x, y, z)$. Using the above derived relationship, one can verify that the Lagrangian time derivative is invariant with respect to the coordinate transformation in (2.1); that is, $d_{t'} = d_t$, where $d_{t'} \equiv \partial_{t'} + \mathbf{u}' \cdot \nabla' + w'\partial_{z'}$ is the Lagrangian time derivative expressed in $(x', y', z', t')$. One can also verify that the anelastic mass continuity equation has the following invariant form in $(x', y', z', t')$:

$$\nabla' \cdot (\rho_a \mathbf{u}') + \partial_{z'}(\rho_a w') = 0, \tag{2.3}$$

where $\rho_a$ is the basic-state air density scaled by its value at $z' = 0$, so $\rho_a$ is a function of $z'$ $(=z)$ only and $\rho_a = 1$ at $z' = 0$.

In the moving coordinate system $(x', y', z', t')$, the temporal variations of VF should be relatively slow (in comparison with variations observed in the local Earth's coordinate system) and thus can be neglected within a sufficiently short time window, which can be about 5 min for a slowly evolving mesocyclone but should be less than 30 s for a rapidly evolving tornado (Wurman and Kosiba 2018; Kurdzo et al. 2017; Bluestein et al. 2019). For the method formulated in this paper, the analysis time window is the time period of radar volume (or sector) scan, which is about 5 min for a volume scan from an operational WSR-88D but can be shorter than 10 s for a sector scan from a rapid-scan mobile radar (see Table 1 of Kurdzo et al. 2017). As the method is formulated for analyzing the time averaged VF over each analysis time window, $\mathbf{u}' + w'\mathbf{e}_3$ is treated as a stationary vector field within each analysis time window in $(x', y', z', t')$ and therefore can only vary with time between consecutive analysis time windows (although $\mathbf{u}_v + w\mathbf{k} = \mathbf{u}' + w'\mathbf{x}_{cz} + w'\mathbf{k}$ can vary with time within each analysis time window due to the continuous variation of $\mathbf{x}_{cz}$ with time). Thus, the temporal resolution of analyzed VFs depends on the radar volume (or sector) scan rate over the concerned tornadic mesocyclone.

### b. VF partition and partitioned analyses

Since the vortex is centered at the origin of $(x', y')$ for any given $(z', t')$, we can transform $(x', y', z')$ to a vortex-following cylindrical coordinate system $(R, \beta, z')$, where

$$R \equiv (x'^2 + y'^2)^{1/2}, \quad (x', y') = R(\cos\beta, \sin\beta). \tag{2.4}$$

In $(R, \beta, z')$, $\mathbf{u}' = u'\mathbf{i} + v'\mathbf{j}$ can be expressed by $\mathbf{u}' = V_R\mathbf{r}_c + V_T\mathbf{t}_c$, where $\mathbf{r}_c$ (or $\mathbf{t}_c$) is the unit vector along the radial (or tangential) direction with respect to the vortex center, and $V_R$ (or $V_T$) is the radial (or tangential) component of $\mathbf{u}'$. Thus, the VF expressed by $\mathbf{u}' + w'\mathbf{e}_3 = V_R\mathbf{r}_c + V_T\mathbf{t}_c + w'\mathbf{e}_3$ in $(R, \beta, z')$ can be partitioned into an axisymmetric part, denoted by $\mathbf{u}^s + w^s\mathbf{e}_3 = V_R^s\mathbf{r}_c + V_T^s\mathbf{t}_c + w^s\mathbf{e}_3$, and an asymmetric part, denoted by $\mathbf{u}^a + w^a\mathbf{e}_3 = V_R^a\mathbf{r}_c + V_T^a\mathbf{t}_c + w^a\mathbf{e}_3$, where $(V_R^s, V_T^s, w^s) \equiv (2\pi)^{-1}\int_{-\pi}^{\pi}(V_R, V_T, w')\,d\beta$ and $(V_R^a, V_T^a, w^a) \equiv (V_R, V_T, w') - (V_R^s, V_T^s, w^s)$. Substituting this partition into (2.2) gives the axisymmetric and asymmetric parts of $\mathbf{u}_v + w\mathbf{k}$ defined in the forms of $\mathbf{u}_s + w_s\mathbf{k} \equiv \mathbf{u}^s + w^s\mathbf{x}_{cz} + w^s\mathbf{k}$ and $\mathbf{u}_a + w_a\mathbf{k} \equiv \mathbf{u}^a + w^a\mathbf{x}_{cz} + w^a\mathbf{k}$, respectively. Here, by using the subscript $s$ (or $a$), $\mathbf{u}_s$ (or $\mathbf{u}_a$) denotes the axisymmetric (or asymmetric) part of $\mathbf{u}_v$, while by using the superscript s (or a), $\mathbf{u}^s$ (or $\mathbf{u}^a$) denotes the axisymmetric (or asymmetric) part of $\mathbf{u}'$. Similarly, $w_s$ (or $w_a$) denotes the axisymmetric (or asymmetric) part of $w$, while $w^s$ (or $w^a$) denotes the axisymmetric (or asymmetric) part of $w'$. Note that $w = w'$ in (2.2), so $w_s = w^s$ and $w_a = w^a$. Note also that $\mathbf{e}_3 = \mathbf{x}_{cz} + \mathbf{k}$ (see Fig. 1b), so $\mathbf{u}_s + w_s\mathbf{k} \equiv \mathbf{u}^s + w^s\mathbf{x}_{cz} + w^s\mathbf{k} = \mathbf{u}^s + w^s\mathbf{e}_3$ and $\mathbf{u}_a + w_a\mathbf{k} \equiv \mathbf{u}^a + w^a\mathbf{x}_{cz} + w^a\mathbf{k} = \mathbf{u}^a + w^a\mathbf{e}_3$. A list of frequently used variables and expressions defined and introduced in this section is given in Table 1.

The VF expressed by $\mathbf{u}_v + w\mathbf{k}$ in $(x, y, z)$ can be also expressed by $v_R\mathbf{r}_c + v_T\mathbf{t}_c + w\mathbf{k}$, where $v_R \equiv \mathbf{u}_v \cdot \mathbf{r}_c = V_R + w\mathbf{x}_{cz} \cdot \mathbf{r}_c$ and $v_T \equiv \mathbf{u}_v \cdot \mathbf{t}_c = V_T + w\mathbf{x}_{cz} \cdot \mathbf{t}_c$. Using this expression, the axisymmetric part of the 2D vortex wind can be defined by $(v_R^s, v_T^s) \equiv (2\pi)^{-1}\int_{-\pi}^{\pi}(v_R, v_T)\,d\beta$, which is different from $(V_R^s, V_T^s)$ defined above unless $\mathbf{x}_{cz} = 0$. This definition is convenient for analyzing 2D horizontal vortex winds as it does not require $w'\mathbf{e}_3$ be also analyzed. Because of this, this definition has been commonly used, either explicitly or implicitly, in previously developed methods for simulating and/or detecting tornadic vortex signatures from radar observations (Wood and Brown 1997, 2011; Stumpf et al. 1998; Liu et al. 2007; Newman et al. 2013) and for analyzing vortex winds in radar-observed tornadic mesocyclones (Lee and Wurman 2005; Potvin et al. 2009, 2011; Xu et al. 2015b). In this case, the projection of $w'\mathbf{e}_3$ on $\mathbf{r}_c$ (or $\mathbf{t}_c$), that is, $w\mathbf{x}_{cz} \cdot \mathbf{r}_c$ (or $w\mathbf{x}_{cz} \cdot \mathbf{t}_c$) is included in $v_R = V_R + w\mathbf{x}_{cz} \cdot \mathbf{r}_c$ (or $v_T = V_T + w\mathbf{x}_{cz} \cdot \mathbf{t}_c$), so $v_R^s$ (or $v_T^s$) contains the azimuthally averaged value of $w\mathbf{x}_{cz} \cdot \mathbf{r}_c$ (or $w\mathbf{x}_{cz} \cdot \mathbf{t}_c$) which is generally nonzero and can be large inside a slantwise updraft or downdraft along the vortex core. Thus, $(v_R^s, v_T^s, w^s)$ and its related vortex wind partition are not suitable for 3D VF analyses in $(x', y', z')$. Besides, unlike $(V_R^s, w^s)$, $(v_R^s, w^s)$ cannot be expressed succinctly by a single scalar to satisfy the continuity equation in $(R, z')$ [see (3.1)–(3.2)] and also, unlike $(V_R^a, V_T^a, w^a)$, $(v_R^a, v_T^a, w^a) \equiv (v_R, v_T, w) - (v_R^s, v_T^s, w^s)$ cannot be expressed succinctly by two scalars [see (4.1)] to satisfy the continuity equation in $(x', y', z')$.

As mentioned in the introduction, the two parts of VF can be analyzed either jointly in a single step or separately in two steps with the axisymmetric part analyzed in the first step. Since the formulations for analyzing the two parts will be derived separately in sections 3 and 4, it is convenient to present the analysis method in two steps. In this case, the first step analyzes the axisymmetric part of VF [that is, $(\mathbf{u}^s, w^s)$ in $(R, \beta, z')$ or, equivalently, $(\mathbf{u}_s, w_s) = (\mathbf{u}^s + w^s\mathbf{x}_{cz}, w^s)$ in $(x, y, z, t)$] with the background wind given by $\mathbf{u}_c$ and the radial-velocity innovation (i.e., observation minus background at each observation location) given by

$$v_r^i = v_r^o - w_T \sin\theta - \mathbf{r}_o \cdot \mathbf{u}_c, \tag{2.5}$$

where $v_r^o$ denotes the radar-observed radial velocity, $w_T\,(<0)$ is the downward terminal velocity of hydrometeors, $\theta$ is the slope angle of radar beam relative to the Earth surface beneath the observation point, and $\mathbf{r}_o$ is the unit vector in the radar beam direction. The second step analyzes the remaining asymmetric

TABLE 1. List of frequently used variables and expressions defined and introduced in section 2.

| Variable/expression | Description |
|---|---|
| $(\mathbf{e}_1, \mathbf{e}_2, \mathbf{e}_3)$ | Covariant basis vectors in $(x', y', z')$; see Fig. 1b |
| $(\mathbf{i}, \mathbf{j}, \mathbf{k})$ | Unit vectors in $(x, y, z)$ directions |
| $(R, \beta)$ | Polar coordinate system transformed from $(x', y')$ in (2.4) |
| $\mathbf{r}_c$ (or $\mathbf{t}_c$) | Unit vector in radial (or tangential) direction along $R$ (or $\beta$) |
| $\mathbf{r}_o$ | Unit vector in the radar beam direction |
| $\mathbf{u} + w\mathbf{k} \equiv u\mathbf{i} + v\mathbf{j} + w\mathbf{k}$ | 3D vector velocity of the total wind $(u, v, w)$ in $(x, y, z)$ |
| $\mathbf{u}_c \equiv \partial_t \mathbf{x}_c = \partial_t x_c \mathbf{i} + \partial_t y_c \mathbf{j} \equiv u_c \mathbf{i} + v_c \mathbf{j}$ | Vortex center moving velocity |
| $(u_v, v_v, w) \equiv (u - u_c, v - v_c, w)$ | Velocity components of VF in $(x, y, z)$ |
| $\mathbf{u}_v + w\mathbf{k} \equiv u_v \mathbf{i} + v_v \mathbf{j} + w\mathbf{k}$ | 3D vector velocity of VF in $(x, y, z)$ |
| $(u', v', w') \equiv d_t(x', y', z')$ | Contravariant velocity components of VF in $(x', y', z')$ |
| $\mathbf{u}' + w'\mathbf{e}_3 \equiv u'\mathbf{e}_1 + v'\mathbf{e}_2 + w'\mathbf{e}_3$ | 3D vector velocity of VF represented in $(x', y', z')$ |
| $\mathbf{u}^s = V_R^s \mathbf{r}_c + V_T^s \mathbf{t}_c = u^s \mathbf{i} + v^s \mathbf{j}$ | Axisymmetric part of $\mathbf{u}'$ |
| $\mathbf{u}^a = V_R^a \mathbf{r}_c + V_T^a \mathbf{t}_c = u^a \mathbf{i} + v^a \mathbf{j}$ | Asymmetric part of $\mathbf{u}'$ |
| $\mathbf{u}_s + w_s\mathbf{k} \equiv u_s \mathbf{i} + v_s \mathbf{j} + w_s \mathbf{k}$ | Axisymmetric part of $\mathbf{u}_v + w\mathbf{k}$ |
| $\mathbf{u}_a + w_a\mathbf{k} \equiv u_a \mathbf{i} + v_a \mathbf{j} + w_a \mathbf{k}$ | Asymmetric part of $\mathbf{u}_v + w\mathbf{k}$ |
| $V_R$ (or $V_T$) | Radial (or tangential) component of $\mathbf{u}'$ |
| $(V_R^s, V_T^s, w^s)$ | Axisymmetric part of $(V_R, V_T, w')$ |
| $(V_R^a, V_T^a, w^a)$ | Asymmetric part of $(V_R, V_T, w')$ |
| $v_r^i$ (or $v_r^{is}$) | Radial-velocity innovation introduced in (2.5) [or (2.6)] |
| $(x', y', z', t')$ | Moving coordinate system defined in (2.1a) |
| $\mathbf{x}_c \equiv x_c \mathbf{i} + y_c \mathbf{j}$ | Vortex center location as a function of $(z, t)$ |
| $\mathbf{x}_{cz} \equiv \partial_z \mathbf{x}_c = \partial_z x_c \mathbf{i} + \partial_z y_c \mathbf{j} \equiv x_{cz} \mathbf{i} + y_{cz} \mathbf{j}$ | Vertical slope of vortex center axis |
| $\beta$ | See $(R, \beta)$ above |
| $\theta$ | Slope angle of radar beam |
| $\rho_a$ | Basic-state air density scaled by its value at $z = 0$ |

part [that is, $(\mathbf{u}^a, w^a)$ in $(R, \beta, z')$ or, equivalently, $(\mathbf{u}_a, w_a) = (\mathbf{u}^a + w^a \mathbf{x}_{cz}, w^a)$ in $(x, y, z, t)$] with the background wind updated to $\mathbf{u}_c + \mathbf{u}_s + w_s\mathbf{k}$ and the radial-velocity innovations updated to

$$v_r^{is} \equiv v_r^o - w_T \sin\theta - \mathbf{r}_o \cdot (\mathbf{u}_c + \mathbf{u}_s + w_s\mathbf{k}) = v_r^i - \mathbf{r}_o \cdot (\mathbf{u}_s + w_s\mathbf{k}). \tag{2.6}$$

The detailed methods for the aforementioned two steps are described in sections 3 and 4.

### c. *Background error partition and related theoretical considerations*

Consider that $\mathbf{x}_c$ and $\mathbf{u}_c \equiv \partial_t \mathbf{x}_c$ can be estimated accurately (within $\pm 0.2$ km and $\pm 1\ \mathrm{m\,s^{-1}}$ to their respective true values) by using the method of Xu et al. (2017) and $\mathbf{u}_c$ is used as the background wind in $(x, y, z, t)$ for the first-step analysis, then the background wind is zero in $(x', y', z', t')$ and the background error is simply the true VF, that is, the true total wind minus $\mathbf{u}_c$. Thus, qualitative features of background error statistics can be envisioned by considering a hypothetical ensemble of true vortices with no prior information on vortex rotation direction (so the ensemble includes both cyclonic and anticyclonic vortices). When these true vortices are transformed into their respective moving coordinate systems, they become cocentered in $(x', y', z', t')$. In this case, one can envision that these cocentered vortices should have a large ensemble spread with a near-zero mean for the sampled VFs (as their ensemble includes both cyclonic and anticyclonic vortices). However, if the ensemble includes only cyclonic vortices, then their axisymmetric parts should have a large ensemble mean with a relatively small spread. On the other hand, the asymmetric parts of these cocentered vortices should have a small ensemble mean with a relatively large spread in any cases.

Based on the above considerations, the background error statistics for the axisymmetric part can be modeled approximately with zero mean but nonzero variance (or with nonzero mean but zero variance) if both cyclonic and anticyclonic vortices (or only cyclonic vortices) are included in the statistics. Since the variational method is formulated in this paper not only for stand-alone VF analyses [with zero background wind in $(x', y', z', t')$] but also for its potential future applications to vortex wind data assimilation (with background winds from high-resolution model predictions), it is convenient to assume that the background error is unbiased (with zero mean) for not only the asymmetric part but also the axisymmetric part, and this assumption will be revisited in the conclusion section. Furthermore, since the axisymmetric part has no azimuthal variation and the asymmetric part is defined with zero azimuthal mean, the background error correlation between the two parts should be very weak and can be simply neglected. With this simplification, background error covariance functions can be formulated independently for the two parts to avoid the complications and difficulties in deriving or computing the analysis error covariance from the first-step analysis and using it as the background error covariance for the second-step analysis (Xu et al. 2016).

In addition to the above considerations, the VF in $(x', y', z', t')$ should satisfy the following two boundary conditions: (a) $w^s$ and $w^a \to 0$ as $z' \to 0$ (at the lower rigid boundary); (b) $V_R^s, V_T^s, V_R^a,$

$V_T^a$, and $w^a \to 0$ as $R \to 0$ (at the vortex center). Since the true VF represents the background error as explained earlier, the above boundary conditions should be also satisfied by the partitioned background error standard deviations. These boundary conditions will be built into the background error covariance functions formulated in the next two sections.

## 3. Formulations for analyzing the axisymmetric part of VF

### a. Control variables and observation operator

As explained in section 2a, the axisymmetric part of VF, $(\mathbf{u}^s, w^s) = (V_T^s \mathbf{t}_c + V_R^s \mathbf{r}_c, w^s)$, is treated as a stationary vector field in $(x', y', z', t')$ over each analysis time window. With this treatment, $(V_T^s, V_R^s, w^s)$ are functions of $(R, z')$ only and can be substituted into $\mathbf{r}_o \cdot (\mathbf{u}^s + w^s \mathbf{x}_{cz} + w^s \mathbf{k}) = \mathbf{r}_o \cdot (\mathbf{u}_s + w_s \mathbf{k})$ to fit $v_r^i$ [defined in (2.4)] over the analysis time window. In this case, the mass continuity equation, (2.3), reduces to

$$\partial_R(\rho_a R V_R^s) + \partial_{z'}(\rho_a R w^s) = 0. \tag{3.1}$$

Constrained by (3.1), the density-weighted vertical circulation $\rho_a(V_R^s, w^s)$ in $(R, z')$ can be expressed by the cylindrical streamfunction $\psi^s$ defined below:

$$\rho_a R(V_R^s, w^s) \equiv \left(-\partial_{z'} R\psi^s, \partial_R R\psi^s\right), \tag{3.2}$$

where $R\psi^s$ (rather than $\psi^s$) is the classical Stokes streamfunction but defined in the cylindrical coordinate system $(R, z')$ with a slantwise-curved axis in general. The boundary conditions of $w^s = 0$ at $z' = 0$ and $V_R^s = 0$ at $R = 0$ can be satisfied automatically if $\psi^s = 0$ at $z' = 0$ and $R = 0$.

The three components of $(\mathbf{u}_s, w_s) \equiv (\mathbf{u}^s + w^s \mathbf{x}_{cz}, w^s)$, defined in section 2b according to (2.2), can be expressed by the two control variables, $\psi^s$ and $V_T^s$, in the following forms:

$$\begin{aligned} u_s &= -\sin\beta V_T^s - \cos\beta \partial_{z'}\psi^s/\rho_a + x_{cz} w^s, \\ v_s &= \cos\beta V_T^s - \sin\beta \partial_{z'}\psi^s/\rho_a + y_{cz} w^s, \\ w_s &= w^s = \partial_R(R\psi^s)/(\rho_a R). \end{aligned} \tag{3.3}$$

The radial component of $(\mathbf{u}_s, w_s)$ in $(x, y, z, t)$ is then given by

$$v_r \equiv \mathbf{r}_o \cdot (\mathbf{u}_s + w_s \mathbf{k}) = (u_s \sin\varphi + v_s \cos\varphi)\cos\theta + w_s \sin\theta, \tag{3.4}$$

where $\varphi$ is the azimuthal angle (clockwise with respect to the $y$ coordinate pointing to the north) of the concerned observation point viewed from the radar site, and $\theta$ is as in (2.5). The observation operator that relates the control variables $(V_R^s, \psi^s)$ to the innovation $v_r^i$ defined in (2.5) is formulated analytically by (3.3)–(3.4).

### b. Cost function and background error covariance functions

The cost function for fitting $v_r$ in (3.3)–(3.4) to $v_r^i$ in (2.5) is

$$J = \mathbf{a}^{\mathrm{T}} \mathbf{B}^{-1} \mathbf{a} + |\mathbf{H}\mathbf{a} - \mathbf{d}|^2/\sigma_o^2, \tag{3.5}$$

where $\mathbf{a} = (\mathbf{a}_1^{\mathrm{T}}, \mathbf{a}_2^{\mathrm{T}})^{\mathrm{T}}$, $\mathbf{a}_1$ (or $\mathbf{a}_2$) is a column vector to denote the state vector of $V_T^s$ (or $\psi^s$), $\mathbf{B}$ is the background error covariance matrix, $\mathbf{H}$ is the radar radial-velocity observation operator formulated in a matrix form by using (3.3)–(3.4), $\mathbf{d}$ is the innovation vector, that is, the state vector of $v_r^i$ in (2.5), and $\sigma_o$ is the observation error standard deviation. Here, the observation errors are assumed uncorrelated, so the observation error covariance matrix has the diagonal form of $\sigma_o^2 \mathbf{I}$, where $\mathbf{I}$ is the identity matrix in the observation space. Note that the radar radial-velocity observations must be processed through stringent data quality control so their bias errors are largely eliminated, while their random errors are correlated only between neighboring gates and beams according to Xu et al. (2007a,b). Thus, for simplicity, the observation errors can be assumed uncorrelated.

The background errors of $(V_T^s, \psi^s)$ are assumed uncorrelated between the two variables and asymptotically homogeneous and isotropic away from the vortex center and ground surface in $(r, h)$, where

$$\begin{aligned} &r \equiv \operatorname{ar\,sinh}(R/R_c)/l = \ln[(R/R_c + (R^2/R_c^2 + 1)^{1/2}]/l \quad \text{and} \\ &h \equiv z'/H, \end{aligned} \tag{3.6}$$

$R_c$ (=1–2 km) is the radial-length scale of the vortex core resolvable by radar radial-velocity observations, $l$ (or $H$) is the background error decorrelation length (or depth) factored into $r$ (or $h$). Here, $(l, H)$ can be estimated or specified differently for $V_T^s$ and $\psi^s$, so the coordinate transformation from $(R, z')$ to $(r, h)$ in (3.6) can be also different for $V_T^s$ and $\psi^s$. Note that $rl = \operatorname{ar\,sinh}(R/R_c) \approx R/R_c$ for $R < R_c$, so $R_c$ is also the radial range within which $rl = \operatorname{ar\,sinh}(R/R_c)$ becomes nearly linear. Note also that the decorrelation radial length in the original physical space of $R$ is given by $R_c \sinh(rl + l/2) - R_c \sinh(rl - l/2) = 2R_c \cosh(rl)\sinh(l/2) = 2(R^2 + R_c^2)^{1/2} \sinh(l/2)$, which is essentially a linear function of $R$ given by $2R\sinh(l/2)$ for $R \gg R_c$. This linear increase of background error decorrelation radial length with $R$ reflects the linearly increased radial-length scales of turbulent eddies away from the vortex center in true VFs, because the background error is essentially the true VF as explained in section 2c. However, the along-$z'$ vertical-length scales of turbulent eddies in true VFs are constrained by vertical stratifications and VFs' depths independent of $R$, so a constant background error decorrelation height can be assumed and denoted by $H$. This explains the need and physical implication of the coordinate transformation in (3.6) which is introduced to facilitate the constructions of VF-dependent covariance functions later in this and next sections.

The above assumed noncorrelation between the background errors of $V_T^s$ and $\psi^s$ implies that $\mathbf{B}$ has the following block-diagonal form:

$$\mathbf{B} = (\mathbf{B}_1, \mathbf{B}_2)^{\mathrm{diag}}, \tag{3.7}$$

where $\mathbf{B}_1$ (or $\mathbf{B}_2$) is the univariate background error covariance matrix for $\mathbf{a}_1$ (or $\mathbf{a}_2$). The above assumed asymptotical homogeneity and isotropy in $(r, h)$ for the background errors of $(V_T^s, \psi^s)$ allow Gaussian functions be used in $(r, h)$ to model the background error correlations and thus to construct $\mathbf{B}_1$ and $\mathbf{B}_2$ in the following separable forms:

$$B_{1ij} = \sigma_1^2 G_0(r_i, r_j) G(h_i - h_j), \tag{3.8a}$$

$$B_{2ij} = \sigma_2^2 \rho_i \rho_j G_0(r_i, r_j) G_0(h_i, h_j), \tag{3.8b}$$

where $B_{1ij}$ (or $B_{2ij}$) denotes the $ij$th element of $\mathbf{B}_1$ (or $\mathbf{B}_2$) associated with the $i$th and $j$th points at $(r_i, h_i)$ and $(r_j, h_j)$, respectively, $\rho_i$ (or $\rho_j$) denotes the value of $\rho_a$ at the $i$th (or $j$th) point, $\sigma_1$ is a constant used to quantify the background error standard deviation for $V_T^s$, and $\sigma_2$ is another constant used with $\rho_a$ in the form of $\sigma_2\rho_a$ to quantify the background error standard deviation for $\psi^s$ (so the background error standard deviation can be derived for $V_R^s$ largely independent of the spatial variation of $\rho_a$). The two function forms in (3.8) are defined by

$$G_0(\eta_i, \eta_j) \equiv G(\eta_i - \eta_j) - G(\eta_i + \eta_j), \tag{3.9a}$$

$$G(\eta_i - \eta_j) \equiv \exp[-(\eta_i - \eta_j)^2/2], \tag{3.9b}$$

where $\eta_i$ (or $\eta_j$) represents either $r$ or $h$ at the $i$th (or $j$th) point.

Note that $G(\,)$ in (3.9b) is the Gaussian correlation function. This Gaussian function is modified into $G_0(\eta_i, \eta_j)$ in (3.9a) by subtracting its mirror image obtained by mirror-reflecting one of the corrected points, either $\eta_i$ or $\eta_j$, with respect to $\eta = 0$, so the boundary condition of $G_0(\eta_i, \eta_j) = 0$ at $\eta_i = 0$ or $\eta_j = 0$ can be satisfied automatically (see Fig. 2 and section 2c). As shown in the next subsection, this boundary condition is also satisfied by the function form deconvoluted from $G_0(\eta_i, \eta_j)$, so the required boundary conditions of $V_T^s = 0$ and $V_R^s = 0 = 0$ at $r = 0$ and $w^s = 0$ at $h = 0$ can be satisfied automatically by the solution [see (3.17)].

### c. *Square root of background error covariance matrix*

The square root of $\mathbf{B}_1$ (or $\mathbf{B}_2$) can be constructed analytically as shown below. First, as shown in appendix A, the two functions defined in (3.9) can be expressed by the following integrals:

$$G_0(\eta_i, \eta_j) = \int_0^\infty P_0(\eta_i, \eta_s) P_0(\eta_s, \eta_j)\, d\eta_s, \tag{3.10a}$$

$$G(\eta_i - \eta_j) = \int_{-\infty}^\infty P_0(\eta_i - \eta_s) P(\eta_s - \eta_j)\, d\eta_s, \tag{3.10b}$$

where

$$P_0(\eta_i, \eta_s) \equiv P(\eta_i - \eta_s) - P(\eta_i + \eta_s), \tag{3.11a}$$

$$P(\eta_i - \eta_s) \equiv (2/\pi)^{1/4} \exp[-(\eta_i - \eta_s)^2]. \tag{3.11b}$$

As shown in (3.10b) and (A1), $G(\,)$ is the self-convolution of $P(\,)$, so $P(\,)$ is deconvoluted $G(\,)$. As shown in (A2)–(A6), $G_0(\,,\,)$ defined in (3.9a) consists of four convolutions obtained by substituting $P_0(\,,\,)$ defined in (3.11a) into the integral on the right-hand side of (3.10a), so $P_0(\,,\,)$ is deconvoluted $G_0(\,,\,)$ in a generalized sense.

Since $(V_T^s, \psi^s)$ will be analyzed in a cuboidal domain co-centered with the vortex in $(x', y', z')$, the two correlated points are confined within the radial range of $R_{\max} = L/\sqrt{2}$ and the vertical range of $D$, where $L$ (≈20 km) is domain width and $D$ (<10 km) is domain height. Thus, $r_i$ and $r_j$ are confined between 0 and $r_{\max} \equiv \text{ar sinh}(R_{\max}/R_c)/l$ and $h_i$ and $h_j$ are confined between 0 and $h_{\max} \equiv D/H$. Note that the integrand $P_0(\eta_i, \eta_s)$ $P_0(\eta_s, \eta_j)$ in (3.10a) becomes negligibly small as $\eta_s > \eta_{\max} + 2$ for $\eta_i$ and $\eta_j$ confined between 0 and $\eta_{\max}$, so the range of integration for the integral in (3.10a) can be reduced from $0 \le \eta_s < \infty$ to $0 \le \eta_s \le \eta_{\max} + 2$, where $\eta_{\max} = r_{\max}$ (or $h_{\max}$) if $\eta$ represents $r$ (or $h$). Thus, if $\eta$ represents $r$, the integral in (3.10a) can be discretized into the following form:

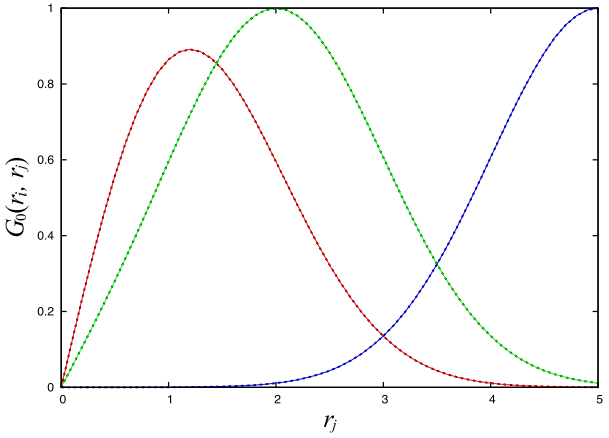


FIG. 2. Constructed $G_0(r_i, r_j)$ [see (3.12a)] plotted as functions of $r_j$ by red, green, and blue curves for $r_i = 1$, 2, and 5, respectively, vs their benchmark truths [see (3.9a)] plotted by black dotted curves.

$$G_0(r_i, r_j) \approx \sum_{0s'} P_0(r_i, r_{s'}) P_0(r_{s'}, r_j) \Delta r = \sum_{0s'} P_{0is'} P_{0s'j}, \tag{3.12a}$$

where $P_{0is'} \equiv P_0(r_i, r_{s'})(\Delta r)^{1/2}$, $P_{0s'j} \equiv P_0(r_{s'}, r_j)(\Delta r)^{1/2}$, $\Delta r$ is the grid spacing of discretized $r_{s'} = (s' + 1/2)\Delta r$, $\sum_{0s'}$ denotes the summation over integer $s'$ from 0 to $S_r \equiv \text{Int}[(r_{\max} + 2)/\Delta r]$, and Int[()] denotes the nearest integer of ( ). To adequately resolve $P_0(r_i, r_{s'})$, $\Delta r$ should not exceed 1/2. As shown in Fig. 2, $G_0(r_i, r_j)$ can be constructed quite accurately by using (3.12a) with $\Delta r = 1/2$.

Similarly, if $\eta$ represents $h$, the integral in (3.10a) can be discretized into

$$G_0(h_i, h_j) \approx \sum_{0s''} P_{0is''} P_{0s''j}, \tag{3.12b}$$

where $P_{0is''} \equiv P_0(h_i, h_{s''})(\Delta h)^{1/2}$, $P_{0s''j} \equiv P_0(h_{s''}, h_j)(\Delta h)^{1/2}$, $\Delta h$ is the grid spacing of discretized $h_{s''} = (s'' + 1/2)\Delta h$, and $\sum_{0s''}$ denotes the summation over integer $s''$ from 0 to $S_h \equiv \text{Int}[(h_{\max} + 2)/\Delta h]$. Also, when $\eta$ represents $h$, the integrand $P(h_i - h_s)P(h_s - h_j)$ in (3.10b) becomes negligibly small as $h_s > h_{\max} + 2$ or $h_s < -2$, so the integration range can be reduced from $-\infty \le h_s < \infty$ to $-2 \le h_s \le h_{\max} + 2$ and the integral in (3.10b) can be discretized into

$$G(h_i - h_j) \approx \sum_{s''} P_{is''} P_{s''j}, \tag{3.12c}$$

where $P_{is''} \equiv P(h_i - h_{s''})(\Delta h)^{1/2}$, $P_{s''j} \equiv P(h_{s''} - h_j)(\Delta h)^{1/2}$, and $\sum_{s''}$ denotes the summation over integer $s''$ from $-\text{Int}[2/\Delta h]$ to $S_h$. To adequately resolve $P_0(h_i, h_{s''})$ and $P(h_i - h_{s''})$, $\Delta h$ should not exceed 1/2. Using (3.12c) with $\Delta h = 1/2$, $G(h_i - h_j)$ can be constructed also quite accurately (not shown but the accuracies are essentially the same as those shown in Fig. 2).

Substituting (3.12) into (3.8) gives

$$B_{1ij} = \sigma_1^2 \sum_s P_{1is} P_{1sj}, \tag{3.13a}$$

$$B_{2ij} = \sigma_2^2 \rho_i \rho_j \sum_{0s} P_{2is} P_{2sj}, \tag{3.13b}$$

where $P_{1is} \equiv P_{0is'} P_{is''}$, $P_{2is} \equiv P_{0is'} P_{0is''}$, and $\sum_s$ (or $\sum_{0s}$) denotes the summation over integer $s$ with $s$ counting through all the points of $(s', s'')$ in the 2D control-variable domain over the ranges of $0 \le s' \le S_r$ and $-\text{Int}[2/\Delta h] \le s'' \le S_h$ (or $0 \le s'' \le S_h$). The matrix forms of (3.13a) and (3.13b) are

$$\mathbf{B}_1 = \sigma_1^2 \mathbf{P}_1 \mathbf{P}_1^{\mathrm{T}}, \tag{3.14a}$$

$$\mathbf{B}_2 = \sigma_2^2 \mathbf{\Lambda} \mathbf{P}_2 (\mathbf{\Lambda} \mathbf{P}_2)^{\mathrm{T}}, \tag{3.14b}$$

where $\mathbf{\Lambda}$ is an diagonal matrix with its $i$th diagonal element given by $\rho_i$. Substituting (3.14) into (3.7) gives $\mathbf{B} = (\sigma_1 \mathbf{P}_1, \sigma_2 \mathbf{\Lambda} \mathbf{P}_2)^{\text{diag}} (\sigma_1 \mathbf{P}_1^{\mathrm{T}}, \sigma_2 \mathbf{\Lambda} \mathbf{P}_2^{\mathrm{T}})^{\text{diag}}$, so $\mathbf{B}^{1/2} = (\sigma_1 \mathbf{P}_1, \sigma_2 \mathbf{\Lambda} \mathbf{P}_2)^{\text{diag}}$ is a square root of $\mathbf{B}$ satisfying $\mathbf{B}^{1/2} \mathbf{B}^{\mathrm{T}/2} = \mathbf{B}$.

*d. Preconditioned cost function*

Substituting $\mathbf{a} = \mathbf{B}^{1/2} \mathbf{c}$ with $\mathbf{B}^{1/2} = (\sigma_1 \mathbf{P}_1, \sigma_2 \mathbf{\Lambda} \mathbf{P}_2)^{\text{diag}}$ into (3.5) gives

$$J = |\mathbf{c}|^2 + |\mathbf{H}' \mathbf{c} - \mathbf{d}/\sigma_0|^2, \tag{3.15}$$

where $\mathbf{H}' = \sigma_o^{-1} \mathbf{H} \mathbf{B}^{1/2}$ is the $\sigma_o$-scaled radial-velocity observation operator for the transformed control vector $\mathbf{c} = (\mathbf{c}_1^{\mathrm{T}}, \mathbf{c}_2^{\mathrm{T}})^{\mathrm{T}}$, and the two components of $\mathbf{a} = (\mathbf{a}_1^{\mathrm{T}}, \mathbf{a}_2^{\mathrm{T}})^{\mathrm{T}}$ are related to $\mathbf{c}_1$ and $\mathbf{c}_2$ by

$$\mathbf{a}_1 = \sigma_1 \mathbf{P}_1 \mathbf{c}_1, \tag{3.16a}$$

$$\mathbf{a}_2 = \sigma_2 \mathbf{\Lambda} \mathbf{P}_2 \mathbf{c}_2. \tag{3.16b}$$

To facilitate the subsequent derivations, the matrix elements in (3.16) are given explicitly by

$$V_T^s(r_i, h_i) = \sigma_1 \sum_s P_{1is} c_{1s}, \tag{3.17a}$$

$$\psi^s(r_i, h_i) = \sigma_2 \rho_i \sum_s P_{2is} c_{2s}, \tag{3.17b}$$

where $(r_i, h_i)$ denotes the $i$th point in $(r, h)$, $c_{1s}$ (or $c_{2s}$) denotes the $s$th element of $\mathbf{c}_1$ (or $\mathbf{c}_2$), and $P_{1is}$ (or $P_{2is}$) is defined in (3.13a) [or (3.13b)].

Substituting (3.17b) into (3.2) gives

$$V_R^s(r_i, h_i) = -\sigma_2 \sum_{0s} U_{is} c_{2s}, \tag{3.18a}$$

$$w^s(r_i, h_i) = \sigma_2 \sum_{0s} W_{is} c_{2s}, \tag{3.18b}$$

where

$$U_{is} = P_0(r_i, r_s)[P_0'(h_i, h_s)/H + P_0(h_i, h_s)(d_z \ln \rho_a)_i](\Delta r \Delta h)^{1/2},$$

$$W_{is} = [P_0'(r_i, r_s) dr/dR_i + P_0(r_i, r_s)/R_i] P_0(h_i, h_s)(\Delta r \Delta h)^{1/2},$$

$$P_0'(r_i, r_s) \equiv \partial P_0(r_i, r_s)/\partial r_i = 2(2/\pi)^{1/4} \left\{ (r_i + r_s) \exp\left[-(r_i + r_s)^2\right] - (r_i - r_s) \exp\left[-(r_i - r_s)^2\right] \right\},$$

$$P_0'(h_i, h_s) \equiv \partial P_0(h_i, h_s)/\partial h_i = 2(2/\pi)^{1/4} \left\{ (h_i + h_s) \exp\left[-(h_i + h_s)^2\right] - (h_i - h_s) \exp\left[-(h_i - h_s)^2\right] \right\},$$

$$dr/dR_i = 1 \Big/ \left[ (R_c^2 + R_i^2)^{1/2} l \right],$$

and $(d_z \ln \rho_a)_i$ denotes the value of $d(\ln \rho_a)/dz$ at the height of the $i$th point.

One can verify that $P_{1is} \to 0$, $U_{is} \to 0$, and $W_{is} \to 2P_0'(0, r_s)(R_c l)^{-1} P_0(h_i, h_s)(\Delta r \Delta h)^{1/2}$ as $r_i \to 0$, and $W_{is} \to 0$ as $h_i \to 0$, so the required boundary conditions of $V_T^s = 0$ and $V_R^s = 0$ at $R = 0$ and $w^s = 0$ at $z' = 0$ (see section 2c) are satisfied automatically by the solutions constructed in (3.17)–(3.18). One can also verify that $\partial W_{is}/\partial R_i \to 0$ as $R_i \to 0$, so $w^s$ is smooth (with no cusp) at $R = 0$.

Substituting (3.17)–(3.18) into (3.3) gives

$$u_s(r_i, h_i, \beta_i, t') = -\sigma_1 \sin\beta_i \sum_s P_{1is} c_{1s} - \sigma_2 \cos\beta_i \sum_{0s} U_{is} c_{2s} + x_{czi} w_s(r_i, h_i), \tag{3.19a}$$

$$v_s(r_i, h_i, \beta_i, t') = \sigma_1 \cos\beta_i \sum_s P_{1is} c_{1s} - \sigma_2 \sin\beta_i \sum_{0s} U_{is} c_{2s} + y_{czi} w_s(r_i, h_i), \tag{3.19b}$$

$$w_s(r_i, h_i) = w^s(r_i, h_i) = \sigma_2 \sum_{0s} W_{is} c_{2s}, \tag{3.19c}$$

where $(r_i, h_i, \beta_i)$ denotes the $i$th point in $(r, h, \beta)$, and $x_{czi} \equiv x_{cz}(z_i, t)$ [or $y_{czi} \equiv y_{cz}(z_i, t)$] denotes the value of $x_{cz}$ (or $y_{cz}$) at $(z_i, t)$ for any $t$ within the analysis time window or for $t$ at the time of the $i$th observation if $(r_i, h_i, \beta_i, t')$ denotes the $i$th observation point. Note that $w_s$ is independent of $(\beta, t')$, so its value at the $i$th point in $(r, h, \beta)$ is simply denoted by $w_s(r_i, h_i)$.

Substituting (3.19) into (3.4) gives

$$v_r(r_i, h_i, \beta_i, t') = \sigma_1 \sum_s T_{is} c_{1s} + \sigma_2 \sum_s R_{is} c_{2s}, \tag{3.20}$$

where

$$T_{is} \equiv \cos\theta_i \cos(\varphi_i + \beta_i) P_{1is},$$

$$R_{is} \equiv [\cos\theta_i (x_{czi} \sin\varphi_i + y_{czi} \cos\varphi_i) + \sin\theta_i] W_{is} - \cos\theta_i \sin(\varphi_i + \beta_i) U_{is}.$$

Here, $\mathbf{H}' = \sigma_o^{-1} \mathbf{H} \mathbf{B}^{1/2}$ is derived analytically in the form of $\mathbf{H}' = (\sigma_1 \mathbf{T}, \sigma_2 \mathbf{R})/\sigma_o$ with the $is$th element of $\mathbf{T}$ (or $\mathbf{R}$) given by $T_{is}$ (or $R_{is}$).

For the axisymmetric part of VF, the dimension of $\mathbf{c}$ can be relatively small ($\le 10^3$), so the minimizer of $J$ in (3.15) can be found by directly solving $\nabla_{\mathbf{c}} J = \mathbf{c} + \mathbf{H}'^{\mathrm{T}} \mathbf{H}' \mathbf{c} - \mathbf{H}'^{\mathrm{T}} \mathbf{d}/\sigma_o = 0$,

which gives $\mathbf{c} = [\mathbf{I} + \mathbf{H'}^{\mathrm{T}}\mathbf{H'}]^{-1}\mathbf{H'}^{\mathrm{T}}\mathbf{d}/\sigma_o$. In particular, since $\mathbf{I} + \mathbf{H'}^{\mathrm{T}}\mathbf{H'}$ is a symmetric matrix, its eigenvalues and eigenvectors can be computed efficiently and used to construct the inverse matrix $[\mathbf{I} + \mathbf{H'}^{\mathrm{T}}\mathbf{H'}]^{-1}$. A list of frequently used variables defined and introduced in this section is given in Table 2.

## 4. Formulations for analyzing the asymmetric part of VF

### a. Control variables and observation operator

As explained in section 2a, the asymmetric part of VF, $(\mathbf{u}^a, w^a)$, is also treated as a stationary vector field in $(x', y', z', t')$ over each analysis time window. With this treatment, $(\mathbf{u}^a, w^a)$ are functions of $(x', y', z')$ or $(R, \beta, z')$ only and can be substituted into $\mathbf{r}_o \cdot (\mathbf{u}^a + w^a\mathbf{x}_{cz} + w^a\mathbf{k}) = \mathbf{r}_o \cdot (\mathbf{u}_a + w_a\mathbf{k})$ to fit $v_r^{\mathrm{is}}$ [defined in (2.6)] over the analysis time window. In this case, the two components of $\rho_a\mathbf{u}^a = (\rho_a u^a, \rho_a v^a)$ can be expressed in $(x', y', z')$ by

$$\rho_a u^a = \partial_{x'}\chi - \partial_{y'}\psi \quad \text{and} \quad \rho_a v^a = \partial_{y'}\chi + \partial_{x'}\psi, \tag{4.1}$$

where $\chi$ (or $\psi$) is the velocity potential (or streamfunction) associated with $\rho_a\mathbf{u}^a$. Using (4.1), $\mathbf{u}^a$ can be partitioned into $\mathbf{u}^a = \mathbf{u}^{\mathrm{ad}} + \mathbf{u}^{\mathrm{ar}}$ with $\rho_a\mathbf{u}^{\mathrm{ad}} \equiv \nabla'\chi$ and $\rho_a\mathbf{u}^{\mathrm{ar}} \equiv \mathbf{k} \times \nabla'\psi$ for the divergent and rotational parts of $\rho_a\mathbf{u}^a$, respectively. In $(R, \beta, z')$, $\mathbf{u}^a$ can be expressed by $\mathbf{u}^a = V_R^a\mathbf{r}_c + V_T^a\mathbf{t}_c$, where $V_R^a$ and $V_T^a$ are the radial and tangential components of $\mathbf{u}^a$, respectively, given by the following partitioned forms:

$$\begin{aligned} V_R^a &= V_R^{\mathrm{ad}} + V_R^{\mathrm{ar}} \equiv (\partial_R\chi - R^{-1}\partial_\beta\psi)/\rho_a, \\ V_T^a &= V_T^{\mathrm{ad}} + V_T^{\mathrm{ar}} \equiv (R^{-1}\partial_\beta\chi + \partial_R\psi)/\rho_a. \end{aligned} \tag{4.2}$$

The mass continuity equation for the asymmetric part has the same form as that for $(\mathbf{u}', w')$ in (2.3). Substituting (4.1) into this mass continuity equation gives $\partial_{z'}(\rho_a w^a) = -\nabla'^2\chi$ in $(x', y', z')$ or, equivalently,

$$\partial_{z'}(\rho_a w^a) = -(R^{-1}\partial_R R\partial_R + R^{-2}\partial_\beta^2)\chi \quad \text{in} \quad (R, \beta, z'). \tag{4.3}$$

The two control variables can be then defined by

$$X \equiv \int_0^{z'} \chi\, dz \quad \text{and} \quad Y \equiv \psi. \tag{4.4}$$

Substituting (4.4) into (4.2)–(4.3) gives

$$\begin{aligned} V_R^a &= (\partial_R\partial_{z'}X - \partial_\beta Y/R)/\rho_a, \\ V_T^a &= (\partial_\beta\partial_{z'}X/R + \partial_R Y)/\rho_a. \\ w^a &= -(\partial_R X/R + \partial_R^2 X + \partial_\beta^2 X/R^2)/\rho_a. \end{aligned} \tag{4.5}$$

Note that $\mathbf{u}^a = u^a\mathbf{i} + v^a\mathbf{j} = V_R^a\mathbf{r}_c + V_T^a\mathbf{t}_c$, so $u^a = V_R^a\mathbf{r}_c \cdot \mathbf{i} + V_T^a\mathbf{t}_c \cdot \mathbf{i} = V_R^a\cos\beta - V_T^a\sin\beta$ and $v^a = V_R^a\mathbf{r}_c \cdot \mathbf{j} + V_T^a\mathbf{t}_c \cdot \mathbf{j} = V_R^a\sin\beta + V_T^a\cos\beta$. Substituting these relationships into $(\mathbf{u}_a, w_a) \equiv (\mathbf{u}^a + w^a\mathbf{x}_{cz}, w^a)$, defined in section 2b according to (2.2), gives

$$\begin{aligned} u_a &= V_R^a\cos\beta - V_T^a\sin\beta + x_{cz}w^a, \\ v_a &= V_R^a\sin\beta + V_T^a\cos\beta + y_{cz}w^a, \\ w_a &= w^a. \end{aligned} \tag{4.6}$$

TABLE 2. List of frequently used variables defined and introduced in section 3.

| Variable | Description |
|---|---|
| $\mathbf{a}$ | State vector of control variables |
| $\mathbf{a}_1$ (or $\mathbf{a}_2$) | State vector of $V_T^s$ (or $\psi^s$) |
| $\mathbf{B}$ | Background error covariance matrix |
| $\mathbf{B}_1$ (or $\mathbf{B}_2$) | Background error covariance matrix for $\mathbf{a}_1$ (or $\mathbf{a}_2$) |
| $B_{1ij}$ (or $B_{2ij}$) | $ij$th element of $\mathbf{B}_1$ (or $\mathbf{B}_2$) |
| $\mathbf{c}$ | Control vector transformed from $\mathbf{a}$ |
| $\mathbf{c}_1$ (or $\mathbf{c}_2$) | Control vector transformed from $\mathbf{a}_1$ (or $\mathbf{a}_2$) |
| $c_{1s}$ (or $c_{2s}$) | $s$th element of $\mathbf{c}_1$ (or $\mathbf{c}_2$) |
| $G_0(,)$ and $G(\ )$ | Function forms defined in (3.9a) and (3.9b) |
| $\mathbf{H'}$ | $\sigma_o$-scaled radial-velocity observation operator for $\mathbf{c}$ |
| $h \equiv z'/H$ | $z'$ scaled by background error decorrelation depth $H$ |
| $\Delta h$ | Grid spacing of $h$ for constructing the space of $\mathbf{c}$ |
| $l$ | Background error decorrelation length factored in $r$ |
| $P_0(,)$ and $P(\ )$ | Function forms defined in (3.11a) and (3.11b) |
| $\mathbf{P}_1$ (or $\mathbf{P}_2$) | Matrix introduced in (3.14a) [or (3.14b)] |
| $P_{1is}$ (or $P_{2is}$) | $is$th element of $\mathbf{P}_1$ (or $\mathbf{P}_2$) |
| $R_c$ | Radial-length scale of vortex core |
| $r = \mathrm{ar\,sinh}(R/R_c)/l$ | Transformed radial distance: $\mathrm{ar\,sinh}(R/R_c)$ scaled by $l$ |
| $\Delta r$ | Grid spacing of $r$ for constructing the space of $\mathbf{c}$ |
| $\mathbf{R}$ (or $\mathbf{T}$) | Matrix defined in (3.20) |
| $R_{is}$ (or $T_{is}$) | $is$th element of $\mathbf{R}$ (or $\mathbf{T}$) |
| $\mathbf{\Lambda}$ | Diagonal matrix with its $i$th diagonal element given by $\rho_i$ |
| $\rho_i$ | Value of $\rho_a$ at $i$th point |
| $\sigma_1$ (or $\sigma_2$) | Background error standard deviation for $V_T^s$ (or $\psi^s/\rho_a$) |
| $\psi^s$ | Cylindrical streamfunction defined in (3.2) |

The radial component of $\mathbf{u}_a + w_a\mathbf{k}$ in $(x, y, z, t)$ is then given by

$$v_r \equiv \mathbf{r}_o \cdot (\mathbf{u}_a + w_a\mathbf{k}) = (u_a\sin\varphi + v_a\cos\varphi)\cos\theta + w_a\sin\theta. \tag{4.7}$$

The observation operator that relates the control variables $(X, Y)$ to the updated radial-velocity innovations $v_r^{\mathrm{is}}$ defined in (2.6) is thus formulated by (4.6)–(4.7).

### b. Cost function and background error covariance functions

The cost function for fitting $v_r$ in (4.6)–(4.7) to $v_r^{\mathrm{is}}$ in (2.6) has the same matrix form as that in (3.5), except that $\mathbf{a} = (\mathbf{a}_3^{\mathrm{T}}, \mathbf{a}_4^{\mathrm{T}})^{\mathrm{T}}$, $\mathbf{a}_3$ (or $\mathbf{a}_4$) is the state vector of $X$ (or $Y$), $\mathbf{H}$ is the observation operator formulated in (4.6)–(4.7), $\mathbf{d}$ becomes the state vector of $v_r^{\mathrm{is}}$ for the updated radial-velocity innovations in (2.6), $\mathbf{B} = (\mathbf{B}_3, \mathbf{B}_4)^{\mathrm{diag}}$, and $\mathbf{B}_3$ (or $\mathbf{B}_4$) is the univariate background error covariance matrix for $\mathbf{a}_3$ (or $\mathbf{a}_4$). The background errors of $(X, Y)$ are assumed to be uncorrelated between the two variables and become increasingly homogeneous and isotropic away from the vortex center and ground surface in $(r, \phi, h)$, where $\phi = \beta/\Phi$, $\Phi$ is a function of $R$ introduced later in (4.9) to

quantify the decorrelation arc along $\beta$, ($r$, $h$) is transformed from ($R$, $z'$) according to (3.6) and the transformed ($r$, $h$) depend on ($l$, $H$) that can be estimated or specified differently for $X$ and $Y$. In addition, since the true ($V_R^a$, $V_T^a$, $w^a$) diminish to zero at the vortex center and so do their represented background errors, the background error standard deviations of $X$ and $Y$ must decrease to zero rapidly enough as $R \to 0$ to ensure the analyzed ($V_R^a$, $V_T^a$, $w^a$) approach zero at the vortex center and thus to prevent the analyzed asymmetric part of VF from becoming singular or failing to converge at the vortex center (see the last paragraph of appendix C). This is achieved by using a smooth function of $R$, defined by $F \equiv [\tanh(R/R_e)]^2$, to modulate the background error standard deviations of $X$ and $Y$ mainly in the vortex core, where the scaling factor $R_e$ should have the same order of magnitude as $R_c$.

Based on the above considerations, $\mathbf{B}_3$ and $\mathbf{B}_4$ can be constructed by Gaussian functions as shown below:

$$B_{3ij} = \sigma_3^2 \gamma_i \gamma_j G_0(r_i, r_j) G_0(h_i, h_j) C(\beta_i - \beta_j), \tag{4.8a}$$

$$B_{4ij} = \sigma_4^2 \gamma_i \gamma_j G_0(r_i, r_j) G(h_i - h_j) C(\beta_i - \beta_j), \tag{4.8b}$$

where $B_{3ij}$ (or $B_{4ij}$) denotes the $ij$th element of $\mathbf{B}_3$ (or $\mathbf{B}_4$) associated with the $i$th and $j$th points at ($r_i$, $\beta_i$, $h_i$) and ($r_j$, $\beta_j$, $h_j$), respectively, $\gamma_i$ (or $\gamma_j$) denotes the value of $\gamma \equiv \rho_a F$ at the $i$th (or $j$th) point, $\sigma_3$ (or $\sigma_4$) is a constant used with $\gamma$ to quantify the background error standard deviation for $X$ (or $Y$), the function form of $G_0(\,,)$ [or $G(\,)$] is defined in (3.9a) [or (3.9b)], and $C(\beta_i - \beta_j)$ is given by

$$\begin{aligned} C(\beta_i - \beta_j) &= [2\Phi_i\Phi_j/(\Phi_i^2 + \Phi_j^2)]^{1/2} \textstyle\sum_n \exp[-(\beta_i - \beta_j - 2n\pi)^2/(\Phi_i^2 + \Phi_j^2)] \\ &\approx [2\Phi_i\Phi_j/(\Phi_i^2 + \Phi_j^2)]^{1/2} \exp[(-|\beta_i - \beta_j|_{\rm mn})^2/(\Phi_i^2 + \Phi_j^2)] \quad \text{for} \quad \Phi_i \quad \text{and} \quad \Phi_j \le \pi/2, \end{aligned} \tag{4.9}$$

where $\sum_n$ denotes the summation over integer $n$ from 0 to $\pm\infty$, $|\beta_i - \beta_j|_{mn} = \min(|\beta_i - \beta_j|, |\beta_i - \beta_j \pm 2\pi|)$, $\Phi_i$ (or $\Phi_j$) is the value of $\Phi \equiv 2\sinh(l/2) + [\Phi_0 - 2\sinh(l/2)]R_p/(R + R_p)$ at $R = R_i$ (or $R_j$), $R_p$ can be set to $R_p = L/4$ (= 5 km for $L$ = 20 km), and $\Phi_0$ can be set between $\pi/2$ and $\pi$. When the two correlated points are on the same circle or on same cylindrical surface (i.e., $R_i = R_j$), $\Phi_i = \Phi_j$ and (4.9) reduces to

$$\begin{aligned} C(\beta_i - \beta_j) &= \textstyle\sum_n G(\phi_i - \phi_j - 2n\pi/\Phi) \\ &\approx G(|\phi_i - \phi_j|_{\rm mn}) \quad \text{for} \quad \Phi \le \pi/2, \end{aligned}$$

where $\Phi = \Phi_i = \Phi_j$, $\phi_i - \phi_j = (\beta_i - \beta_j)/\Phi$, $|\phi_i - \phi_j|_{mn} = \min(|\phi_i - \phi_j|, |\phi_i - \phi_j \pm 2\pi/\Phi|)$, and $\phi = \beta/\Phi$. In this case, $\Phi$ is the decorrelation arc for the given $R$. Note that $\Phi \to 2\sinh(l/2)$ as $R \to \infty$, so the decorrelation arc length, $R\Phi$, becomes equal to the decorrelation radial length in $R$ as the latter is given by $2(R^2 + R_c^2)^{1/2}\sinh(l/2)$ and approaches $2R\sinh(l/2)$ in the limit of $R \to \infty$ [see (3.6)]. Note also that $\Phi \to \Phi_0$ as $R \to 0$, so the decorrelation arc becomes sufficiently large to suppress spurious rapid azimuthal variations (not resolvable by radar observations) near the vortex center inside the vortex core.

### c. *Square root of background error covariance matrix*

The square root of $\mathbf{B}_3$ (or $\mathbf{B}_4$) can be derived analytically in the same way as shown for $\mathbf{B}_2$ (or $\mathbf{B}_1$) in section 3c. In addition to the two functions defined in (3.9) and expressed by the integrals in (3.10), as shown in appendix B, $C(\beta_i - \beta_j)$ in (4.9) can be expressed by the following integral:

$$C(\beta_i - \beta_j) = \int_{-\pi}^{\pi} P_c(\beta_i - \beta_s) P_c(\beta_s - \beta_j)\, d\beta_s, \tag{4.10}$$

where

$$\begin{aligned} P_c(\beta_i - \beta_s) &\equiv (2/\pi)^{1/4}\Phi_i^{-1/2} \textstyle\sum_n \exp[-(\beta_i - \beta_s - 2n\pi)^2/\Phi_i^2] \\ &\approx (2/\pi)^{1/4}\Phi_i^{-1/2} \exp[-(|\beta_i - \beta_s|_{\rm mn})^2/\Phi_i^2] \quad \text{for} \\ &\quad \Phi_i \le \pi/2. \end{aligned} \tag{4.11}$$

As shown in (4.10) and (B1), $C(\,)$ is the self-convolution of $P_c(\,)$, so $P_c(\,)$ is deconvoluted $C(\,)$.

The integral in (4.10) can be discretized into

$$C(\beta_i - \beta_j) \approx \textstyle\sum_{s'''} P_{cis'''} P_{cs'''j}, \tag{4.12}$$

where $P_{cis'''} \equiv P_c(\beta_i - \beta_{s'''})(\Delta\beta)^{1/2}$, $P_{cs'''j} \equiv P_c(\beta_j - \beta_{s'''})(\Delta\beta)^{1/2}$, $\Delta\beta = \pi/M$ is the grad spacing for discretized $\beta_{s'''} = s'''\Delta\beta$, and $\sum_{s'''}$ denotes the summation over integer $s'''$ from $1 - M$ to $M$. To adequately resolve $P_c(\beta)$, $\Delta\beta$ should not exceed $\Phi_{mn}/2$, so $M$ cannot be smaller than $2\pi/\Phi_{mn}$, where $\Phi_{mn} = \min[\Phi(R)] = \Phi(L/\sqrt{2})$ for $R \le R_{\max} = L/\sqrt{2}$ but $\Phi_{mn} \to 2\sinh(l/2)$ as $R \to \infty$. The truncated form of $P(\beta_i - \beta_s)$ at the last step of (4.11) is used to compute $P_{cis'''}$ when $\Phi_i \le \pi/2$. Using (3.12a) and (4.12), $G_0(r_i, r_j)C(\beta_i - \beta_j)$ can be constructed quite accurately. When the constructed $G_0(r_i, r_j)C(\beta_i - \beta_j)$ is transformed back into the Cartesian coordinate system of ($x'$, $y'$), its contours exhibit strong VF dependencies in the physical space as shown in Fig. 3.

Substituting (3.12) and (4.12) into (4.8) gives

$$B_{3ij} = \sigma_3^2 \gamma_i \gamma_j \textstyle\sum_{0s} P_{3is} P_{3sj}, \tag{4.13a}$$

$$B_{4ij} = \sigma_4^2 \gamma_i \gamma_j \textstyle\sum_{s} P_{4is} P_{4sj}, \tag{4.13b}$$

where $P_{3is} \equiv P_{0is'} P_{0is''} P_{cis'''}$, $P_{4is} \equiv P_{0is'} P_{is''} P_{cis'''}$, and $\sum_{0s}$ (or $\sum_s$) denotes the summation over integer $s$ with $s$ counting through all the points of ($s'$, $s''$, $s'''$) in the 3D control-variable domain over the ranges of $0 \le s' \le S_r$, $0 \le s'' \le S_h$ (or $-\text{Int}[2/\Delta h] \le s'' \le S_h$) and $1 - M \le s''' \le M$. The matrix forms of (4.13a) and (4.13b) are

$$\mathbf{B}_3 = \sigma_3^2 \mathbf{\Gamma} \mathbf{P}_3 (\mathbf{\Lambda} \mathbf{P}_3)^{\rm T}, \tag{4.14a}$$

$$\mathbf{B}_4 = \sigma_4^2 \mathbf{\Gamma} \mathbf{P}_4 (\mathbf{\Lambda} \mathbf{P}_4)^{\rm T}, \tag{4.14b}$$

where $\mathbf{\Gamma}$ is a diagonal matrix with its $i$th diagonal element given by $\gamma_i$. Substituting (4.14) into $\mathbf{B} = (\mathbf{B}_3, \mathbf{B}_4)^{\rm diag}$

gives $\mathbf{B} = (\sigma_3\mathbf{\Lambda P}_3, \sigma_4\mathbf{\Gamma P}_4)^{\text{diag}}(\sigma_3\mathbf{\Gamma P}_3^{\text{T}}, \sigma_4\mathbf{\Gamma P}_4^{\text{T}})^{\text{diag}}$, so $\mathbf{B}^{1/2} = (\sigma_3\mathbf{\Gamma P}_3,\ \sigma_4\mathbf{\Gamma P}_4)^{\text{diag}}$ is a square root of $\mathbf{B}$ satisfying $\mathbf{B}^{1/2}\mathbf{B}^{\text{T}/2} = \mathbf{B}$.

*d. Preconditioned cost function*

Substituting $\mathbf{a} = \mathbf{B}^{1/2}\mathbf{c}$ with $\mathbf{B}^{1/2} = (\sigma_3\mathbf{\Gamma P}_3,\ \sigma_4\mathbf{\Gamma P}_4)^{\text{diag}}$ into the cost function described in section 4b gives a preconditioned cost function in the same matrix form as that in (3.15), but $\mathbf{d}$ is the state vector of $v_r^{\text{is}}$ in (2.6), $\mathbf{H}' = \sigma_o^{-1}\mathbf{H}\mathbf{B}^{1/2}$ is the $\sigma_o$-scaled radial-velocity observation operator for the newly transformed control vector $\mathbf{c} = (\mathbf{c}_3^{\text{T}}, \mathbf{c}_4^{\text{T}})^{\text{T}}$, and the two components of $\mathbf{a} = (\mathbf{a}_3^{\text{T}}, \mathbf{a}_4^{\text{T}})^{\text{T}}$ are related to $\mathbf{c}_3$ and $\mathbf{c}_4$ by

$$\mathbf{a}_3 = \sigma_3\mathbf{\Gamma P}_3\mathbf{c}_3, \tag{4.15a}$$

$$\mathbf{a}_4 = \sigma_4\mathbf{\Gamma P}_4\mathbf{c}_4. \tag{4.15b}$$

To facilitate the subsequent derivations, the matrix elements in (4.15) are given explicitly by

$$X(r_i, h_i, \beta_i) = \sigma_3\gamma_i\textstyle\sum_{0s} P_{3is}c_{3s}, \tag{4.16a}$$

$$Y(r_i, h_i, \beta_i) = \sigma_4\gamma_i\textstyle\sum_{s} P_{4is}c_{4s}, \tag{4.16b}$$

where $(r_i, h_i, \beta_i)$ denotes the $i$th point in $(r, h, \beta)$, $c_{3s}$ (or $c_{4s}$) denotes the $s$th element of $\mathbf{c}_3$ (or $\mathbf{c}_4$), and $P_{3is}$ (or $P_{4is}$) is defined in (4.13a) [or (4.13b)].

Substituting (4.16) into (4.5) and then into (4.6) gives

$$\begin{aligned} u_a(r_i, h_i, \beta_i, t') &= \sigma_3\textstyle\sum_{0s}(\cos\beta_i X_{1is} - \sin\beta_i X_{2is} - x_{czi}X_{3is})c_{3s} - \sigma_4\sum_s(\cos\beta_i Y_{1is} + \sin\beta_i Y_{2is})c_{4s} + x_{cz}w^a,\\ v_a(r_i, h_i, \beta_i, t') &= \sigma_3\textstyle\sum_{0s}(\sin\beta_i X_{1is} + \cos\beta_i X_{2is} - y_{czi}X_{3is})c_{3s} + \sigma_4\sum_s(\cos\beta_i Y_{2is} - \sin\beta_i Y_{1is})c_{4s} + y_{cz}w^a,\\ w_a(r_i, h_i, \beta_i, t') &= -\sigma_3\textstyle\sum_{0s} X_{3is}c_{3s}, \end{aligned} \tag{4.17}$$

where $x_{czi}$ and $y_{czi}$ are as in (3.19), and the five matrix element terms $X_{1is}$, $X_{2is}$, $Y_{1is}$, $Y_{2is}$ and $X_{3is}$ are given in appendix C with the detailed derivation of (4.17). As shown in (C4)–(C8), all the five matrix element terms approach zero as $r_i \to 0$, and $X_{3is} \to 0$ as $h_i \to 0$. Using these results and noting that $u_a = u^a + x_{cz}w^a$, $v_a = v^a + y_{cz}w^a$ and $w_a = w^a$, one can verify that the required boundary conditions of $u^a = 0$ and $v^a = 0$ at $r = 0$, $w^a = 0$ at $h = 0$ or $r = 0$, and the associated consistency conditions of $u_a = x_{cz}w_a$ and $v_a = y_{cz}w_a$ at $r = 0$ are satisfied automatically by the solutions constructed in (4.17).

Substituting (4.17) into (4.7) gives

$$v_r(r_i, h_i, \beta_i, t_i) = \sigma_3\textstyle\sum_{0s} Q_{is}c_{1s} + \sigma_4\sum_s S_{is}c_{2s}, \tag{4.18}$$

where

$$\begin{aligned} Q_{is} &= \cos\theta_i[\sin(\beta_i + \varphi_i)X_{1is} + \cos(\beta_i + \varphi_i)X_{2is}]\\ &\quad - [\cos\theta_i(x_{czi}\sin\varphi_i + y_{czi}\cos\varphi_i) + \sin\theta_i]X_{3is},\\ S_{is} &= \cos\theta_i[\cos(\beta_i + \varphi_i)Y_{2is} - \sin(\beta_i + \varphi_i)Y_{1is}]. \end{aligned}$$

The observation operator $\mathbf{H}' = \sigma_o^{-1}\mathbf{H}\mathbf{B}^{1/2}$ in the preconditioned cost function is thus derived here analytically in the form of $\mathbf{H}' = (\sigma_3\mathbf{Q}, \sigma_4\mathbf{S})/\sigma_o$ with the $i$th element of $\mathbf{Q}$ (or $\mathbf{S}$) given by $Q_{is}$ (or $S_{is}$). A list of frequently used variables introduced in this section is given in Table 3.

For the asymmetric part of VF, the dimension of the control vector $\mathbf{c}$ can be quite large ($\gg 10^3$), so $\mathbf{c}$ may hardly be computed by using the method of matrix inversion described for the axisymmetric part in section 3d. However, the standard conjugate-gradient descending algorithm can be used to minimize the cost function in the space of $\mathbf{c}$ and thus find the minimizer of the cost function.

As mentioned in the introduction, the axisymmetric part of VF can be also analyzed jointly in combination with the asymmetric part in a single step. This can be done simply by combining $(\mathbf{c}_1^{\text{T}}, \mathbf{c}_2^{\text{T}})$ and $(\mathbf{c}_3^{\text{T}}, \mathbf{c}_4^{\text{T}})^{\text{T}}$ into $\mathbf{c} = (\mathbf{c}_1^{\text{T}}, \mathbf{c}_2^{\text{T}}, \mathbf{c}_3^{\text{T}}, \mathbf{c}_4^{\text{T}})^{\text{T}}$. In this case, the preconditioned cost function has the same matrix form as that in (3.15), except that $\mathbf{B}^{1/2}$ is expanded from $\mathbf{B}^{1/2} = (\sigma_1\mathbf{P}_1, \sigma_2\mathbf{\Lambda P}_2)^{\text{diag}}$ to $\mathbf{B}^{1/2} = (\sigma_1\mathbf{P}_1, \sigma_2\mathbf{\Lambda P}_2, \sigma_3\mathbf{\Gamma P}_3, \sigma_4\mathbf{\Gamma P}_4)^{\text{diag}}$ and $\mathbf{H}' = \mathbf{H}\mathbf{B}^{1/2}/\sigma_o$ is expanded from $\mathbf{H}' = (\sigma_1\mathbf{T}, \sigma_2\mathbf{R})/\sigma_o$ to $\mathbf{H}' = (\sigma_1\mathbf{T}, \sigma_2\mathbf{R}, \sigma_3\mathbf{Q}, \sigma_4\mathbf{S})/\sigma_o$, while $\mathbf{d}$ is still the state vector of $v_r^i$ in (2.5). The process of two-step (or single-step) analysis is shown in Fig. 4a (or Fig. 4b). The final solution $\mathbf{u}_v + w\mathbf{k}$ ($= \mathbf{u}_s + w_s\mathbf{k} + \mathbf{u}_a + w_a\mathbf{k}$) obtained by submitting the minimizer into (3.19) and (4.17) is a vector function of $(r_i, h_i, \beta_i, t')$, while $(r_i, h_i, \beta_i)$ can be a continuously varying point in $(r, h, \beta)$ due to the fact that all the matrix element terms in (3.19) and (4.17) are derived analytically from continuous covariance functions. Thus, the analyzed VF is essentially a spatially continuous vector field. A rigorous proof of this can be given by constructing $J$ as a functional in the space of continuous functions similarly to those presented in appendix A of Xu (2019).

## 5. Conclusions

A variational method is formulated in this paper for analyzing 3D VFs of a single vortex (or each individual subvortex separately but not multiple vortices simultaneously) in radar-scanned tornadic mesocyclones. In this method, the vortex center axis [estimated as a continuous function of height and time in the 4D space by the three-step method of Xu et al. (2017)] is used as the vertical coordinate and the analysis domain is centered along this vertical coordinate. The coordinate system is thus time-varying slantwise curvilinear and nonorthogonal in general [see (2.1)]. Analyzing VFs in this coordinate system confronts new challenging issues concerning how to define suitable momentum control variables to satisfy the mass continuity automatically and how to formulate VF-dependent background error covariance functions for these control variables to satisfy the two required boundary conditions (stated at the end of section 2c): (a) zero vertical velocity at the lower rigid boundary and (b) zero cross-axis velocity along the vortex center axis. These issues are addressed with theoretical considerations as the variational method is formulated in this paper. The main results are summarized below:

(i) The VF, defined by the system-relative wind in the aforementioned slantwise-curvilinear moving coordinate system,

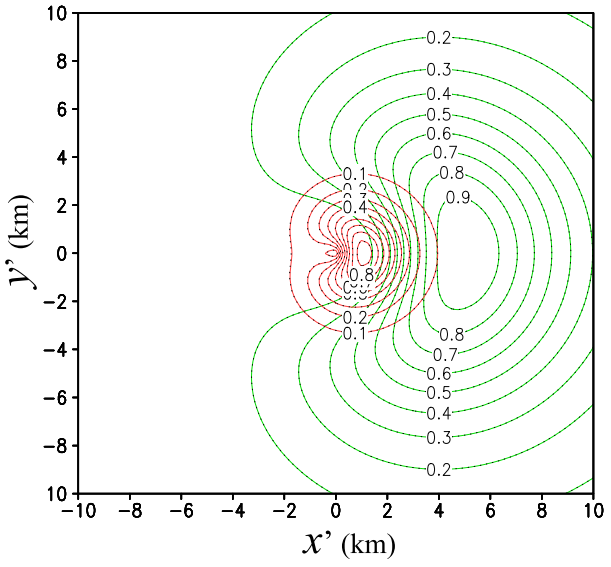


FIG. 3. Constructed $G_0(r_i, r_j)C(\beta_i - \beta_j)$ [see (3.12a) and (4.12)] plotted as functions of $(x', y') = (x'_j, y'_j)$ by red and green contours for $(R_i, \beta_i) = (1\,\text{km}, 0°)$ and $(5\,\text{km}, 0°)$, respectively, vs their benchmark truths [see (3.9a) and (4.9)] plotted by dotted contours with $\Phi_0 = \pi/2$ used in the formulation of $\Phi$ defined in (4.8). Here, $(x'_j, y'_j) = R_c \sinh(r_j l)(\cos\beta_j, \sin\beta_j)$ denotes the $j$th point defined by $(r_j, \beta_j)$ in the $(r, \beta)$-coordinate system but transformed back into the $(x', y')$-coordinate system by using (2.4) and (3.6) with $R_c = 1.5$ km and $l = 1/2$ used in (3.6).

must be expressed in terms of the covariant basis vectors (tangent to the coordinate curves), so the mass continuity equation can be invariant with respect to the coordinate transformation [see (2.1)–(2.3) and section 2a] and the axisymmetric part and remaining asymmetric part of VF can be properly defined (see section 2b) with each part expressed succinctly by two scalar control variables to satisfy the mass continuity equation automatically.

(ii) Azimuthally averaged tangential velocity and cylindrical streamfunction are defined to satisfy the mass continuity equation [see (3.1)–(3.3)] and used as the two scalar control variables in the cost function for analyzing the axisymmetric part of VF [see (3.5)]. Covariance functions are formulated for the two control variables to satisfy the two required boundary conditions by using a Gaussian correlation function (for each control variable along each coordinate) minus its mirror image with respect to the concerned boundary [see (3.9a) and Fig. 2]. These covariance functions are deconvoluted to construct the square root of background error covariance matrix analytically for preconditioning the cost function (see sections 3c and 3d). The deconvoluted covariance functions satisfy the two boundary conditions, so the analyzed axisymmetric part of VF satisfies the two boundary conditions automatically.

(iii) Streamfunction and vertically integrated velocity potential are defined to satisfy the mass continuity equation [see (4.1)–(4.4)] and used as the two scalar control variables in the cost function for analyzing the asymmetric part of VF. VF-dependent correlation functions are formulated for these two control variables [see (4.8) and Fig. 3] to satisfy the required boundary condition (a) by using the approach described in (ii) for the axisymmetric part. To satisfy the required boundary condition (b), the associated background error standard deviations must be modulated along the radial direction in the vortex core so they can diminish rapidly enough toward the vortex center to prevent the analyzed asymmetric part of VF from becoming singular at the vortex center (see appendix C). These VF-dependent covariance functions are deconvoluted to construct the square root of background error covariance matrix to precondition the cost function (see sections 4b–4d). The deconvoluted covariance functions satisfy the two boundary conditions, so the analyzed asymmetric part of VF satisfies the two boundary conditions automatically.

(iv) For each control variable, the background error is assumed to be random with zero mean, asymptotically homogeneous and isotropic away from the vortex center and ground surface in the transformed slantwise cylindrical coordinate system [see (3.6)] in which the error decorrelation radial length (or height) is scaled to a unit value [see (3.8)–(3.9)]. Transformed back to the original physical space, the error decorrelation radial length becomes essentially a linearly increasing function of the radial distance away from the vortex center [see the analysis below (3.6)]. This range-dependent error decorrelation radial length and the range-dependent error decorrelation arc length (see the end of section 4b) reflect the linearly increased horizontal length scales of turbulent eddies away from the vortex center and their correlation structures in true VFs, because the background error is essentially the true VF when the background wind is given by the moving velocity of the vortex center (see section 2c). This explains the necessity and physical implication of the radial coordinate transformation introduced in (3.6).

(v) The axisymmetric part of VF can be analyzed, either separately in the first step or jointly with the asymmetric

TABLE 3. List of frequently used variables defined and introduced in section 4.

| Variable | Description |
|---|---|
| $\mathbf{a}_3$ (or $\mathbf{a}_4$) | State vector of $X$ (or $Y$) |
| $\mathbf{B}_3$ (or $\mathbf{B}_4$) | Background error covariance matrix for $\mathbf{a}_3$ (or $\mathbf{a}_4$) |
| $B_{3ij}$ (or $B_{4ij}$) | $ij$th element of $\mathbf{B}_3$ (or $\mathbf{B}_4$) |
| $\mathbf{c}_3$ (or $\mathbf{c}_4$) | Control vector transformed from $\mathbf{a}_1$ (or $\mathbf{a}_2$) |
| $c_{3s}$ (or $c_{4s}$) | $s$th element of $\mathbf{c}_3$ (or $\mathbf{c}_4$) |
| $C(\,)$ | Function form defined in (4.9) |
| $P_c(\,)$ | Function form defined in (4.11) |
| $\mathbf{P}_3$ (or $\mathbf{P}_4$) | Matrix introduced in (4.14a) [or (4.14b)] |
| $P_{3is}$ (or $P_{4is}$) | $is$th element of $\mathbf{P}_3$ (or $\mathbf{P}_4$) |
| $\mathbf{Q}$ (or $\mathbf{S}$) | Matrix defined in (4.18) |
| $Q_{is}$ (or $S_{is}$) | $is$th element of $\mathbf{Q}$ (or $\mathbf{S}$) |
| $X$ (or $Y$) | Control variable associated with $\chi$ (or $\psi$) defined in (4.4) |
| $\mathbf{\Gamma}$ | Diagonal matrix with its $i$th diagonal element given by $\gamma_i$ |
| $\gamma \equiv \rho_a F$ | Variable introduced in (4.8) with $F \equiv [\tanh(R/R_e)]^2$ |
| $\gamma_i$ | Value of $\gamma$ at $i$th point |
| $\sigma_3$ (or $\sigma_4$) | Background error standard deviation for $X/\gamma$ (or $Y/\gamma$) |
| $\chi$ (or $\psi$) | Velocity potential (or streamfunction) defined in (4.1) for $\rho_a \mathbf{u}^a$ |

(a)

Obtain the axisymmetric part of VF via the following process:
1. Set the innovation vector **d** to the state vector of $v_r^i$ in (2.5).
2. Construct the cost-function in the space of $\mathbf{c} = (\mathbf{c}_1^T, \mathbf{c}_2^T)^T$ by
$$J = |\mathbf{c}|^2 + |\mathbf{H'c} - \mathbf{d}/\sigma_o|^2,$$
where $\mathbf{H'} = (\sigma_1\mathbf{T}, \sigma_2\mathbf{R})/\sigma_o$ with **T** and **R** given in (3.20).
3. Find the minimizer of $J$ by solving for **c** from
$$\nabla_{\mathbf{c}} J = \mathbf{c} + \mathbf{H'}^T\mathbf{H'c} - \mathbf{H'}^T\mathbf{d}/\sigma_o = 0.$$
4. Substitute the minimizer, that is, **c** at the minimum of $J$ into (3.19) to obtain $\mathbf{u}_s + w_s\mathbf{k}$ – the axisymmetric part of VF.

↓

Obtain the asymmetric part of VF via the following process:
1. Set the innovation vector **d** to the state vector of $v_r^{is}$ in (2.6).
2. Construct the cost-function in the space of $\mathbf{c} = (\mathbf{c}_3^T, \mathbf{c}_4^T)^T$ by
$$J = |\mathbf{c}|^2 + |\mathbf{H'c} - \mathbf{d}/\sigma_o|^2,$$
where $\mathbf{H'} = (\sigma_3\mathbf{Q}, \sigma_4\mathbf{S})/\sigma_o$ with **Q** and **S** given in (4.18).
3. Find the minimizer of $J$ by using the standard conjugate-gradient descending algorithm.
4. Substitute the minimizer, that is, **c** at the minimum of $J$ into (4.17) to obtain $\mathbf{u}_a + w_a\mathbf{k}$ – the asymmetric part of VF.

(b)

Obtain the axisymmetric and asymmetric parts of VF jointly via the following process:
1. Set the innovation vector **d** to the state vector of $v_r^i$ in (2.5).
2. Construct the cost-function in $\mathbf{c} = (\mathbf{c}_1^T, \mathbf{c}_2^T, \mathbf{c}_3^T, \mathbf{c}_4^T)^T$ by
$$J = |\mathbf{c}|^2 + |\mathbf{H'c} - \mathbf{d}/\sigma_o|^2,$$
where $\mathbf{H'} = (\sigma_1\mathbf{T}, \sigma_2\mathbf{R}, \sigma_3\mathbf{Q}, \sigma_4\mathbf{S})/\sigma_o$ with **T** and **R** given in (3.20) and **Q** and **S** given in (4.18).
3. Find the minimizer of $J$ by using the standard conjugate-gradient descending algorithm.
4. Substitute the minimizer, that is, **c** at the minimum of $J$ into (3.19) and (4.17) to obtain $\mathbf{u}_s + w_s\mathbf{k}$ and $\mathbf{u}_a + w_a\mathbf{k}$, respectively.

FIG. 4. (a) Process of two-step analysis. (b) Process of single-step analysis.

part in a single step (see the end of section 4d and Fig. 4), although the method is presented in two steps. This makes the method flexible for various applications.

(vi) The temporal resolution of analyzed VFs is limited by the radar volume (or sector) scan rate, because the method is formulated for analyzing the time averaged VF over each analysis time window in the vortex-following moving coordinate system and the analysis time window is updated at the rate of radar volume (or sector) scans that cover the concerned tornadic mesocyclone. On the other hand, the analyzed VF is essentially a spatially continuous vector field (as explained at the end of section 4c), so its spatial resolution can be infinitely high although its intrinsic spatial resolution is limited by the length scale resolvable by the background error correlation functions in connection with spatial distributions of observations.

In this paper, the cost function is formulated in an incremental form and the background error is assumed unbiased (with zero mean). This assumption is made to facilitate future applications (envisioned in the introduction) in which the background winds will be from high-resolution model predictions and the predicted vortices will be recentered to (if not already cocentered with) the true center locations estimated from radar and/or other observations (see condition A stated in the introduction). For a stand-alone VF analysis, the background wind is the estimated vortex center moving velocity and becomes zero in the vortex-following moving coordinate system, so the background error is essentially the true VF. In this case, the background error can be assumed unbiased if cyclonic and anticyclonic vortices are both included in the background error statistics (as explained in section 2b). However, if the (cyclonic or anticyclonic) type of vortex detected from radar observations is used as a priori condition to retain vortices of the observed type only in the statistics, then the conditioned background error statistics for the axisymmetric part of VF will have a large mean with a relatively small variance and thus the background error should be treated mainly as a bias error. In this case, the variational method formulated for analyzing the axisymmetric part of VF in the first step should be considered as a regularized least squares method with the background term reinterpreted as the regularization term, aiming to correct the bias (of the aforementioned zero background wind). The method formulated in this paper has been tested for stand-alone VF analyses with simulated radar observations. The results are presented in Part II (Xu and Wei 2020, manuscript submitted to *J. Atmos. Sci.*).

*Acknowledgments.* The author is thankful to Li Wei at the University of Oklahoma (OU) for producing Figs. 2 and 3, to Vincent Wood at NSSL for reviewing the manuscript internally, and to the anonymous reviewers for their constructive comments and suggestions. The research was supported by the ONR Grants N000141712375 and N000142012449 to OU and the Warn-on-Forecast project at NSSL.

## APPENDIX A

### Derivations of (3.10a) and (3.10b)

Substituting (3.11b) into the integral on the right-hand side of (3.10b) gives

$$\begin{aligned}
&\int_{-\infty}^{\infty} P(\eta_i - \eta_s)P(\eta_s - \eta_j)\,d\eta_s \\
&\quad = (2/\pi)^{1/2}\int_{-\infty}^{\infty} d\eta_s \exp[-(\eta_i - \eta_s)^2 - (\eta_s - \eta_j)^2] \\
&\quad = (2/\pi)^{1/2}\exp[-(\eta_i - \eta_j)^2/2]\int_{-\infty}^{\infty} d\eta_s \exp[-2(\eta_s - \eta_i/2 - \eta_j/2)^2] \\
&\quad = (2/\pi)^{1/2}\exp[-(\eta_i - \eta_j)^2/2]\int_{-\infty}^{\infty} d\eta' \exp(-2\eta'^2) \\
&\quad = \exp[-(\eta_i - \eta_j)^2/2] \equiv G(\eta_i - \eta_j),
\end{aligned} \tag{A1}$$

where $-(\eta_i-\eta_s)^2-(\eta_s-\eta_j)^2=-\eta_i^2-\eta_j^2-2\eta_s^2+2\eta_s(\eta_i+\eta_j)=-\eta_i^2-\eta_j^2-2[\eta_s^2-\eta_s(\eta_i+\eta_j)+(\eta_i+\eta_j)^2/4]+(\eta_i+\eta_j)^2/2=-(\eta_i-\eta_j)^2/2-2(\eta_s-\eta_i/2-\eta_j/2)^2$ is used in the first step, $\eta'=\eta_s-\eta_i/2-\eta_j/2$ is used in the second step, and $\int_{-\infty}^{\infty}d\eta'\exp(-2\eta'^2)=(\pi/2)^{1/2}$, is used in the third step. The result in the last step of (A1) gives the left-hand side of (3.10b).

Changing $\eta_j$ to $-\eta_j$, $\eta_i$ to $-\eta_i$, and $(\eta_i, \eta_j)$ to $(-\eta_i, -\eta_j)$, respectively, in (A1) gives

$$\int_{-\infty}^{\infty}P(\eta_i-\eta_s)P(\eta_s+\eta_j)\,d\eta_s=G(\eta_i+\eta_j),\tag{A2}$$

$$\int_{-\infty}^{\infty}P(\eta_i+\eta_s)P(\eta_s-\eta_j)\,d\eta_s=G(\eta_i+\eta_j),\tag{A3}$$

$$\int_{-\infty}^{\infty}P(\eta_i+\eta_s)P(\eta_s-\eta_j)\,d\eta_s=G(\eta_i-\eta_j),\tag{A4}$$

where the properties that $G(\,)$ defined in (3.9b) and $P(\,)$ defined in (3.11b) are even functions of $(\,)$ are used in the derivations of (A3) and (A4).

Note that $P_0(\eta_i, \eta_s)P_0(\eta_s, \eta_j)$ is an even function of $\eta_s$, so the integral on the right-hand side of (3.10a) can be written into

$$\begin{aligned}\int_{-\infty}^{\infty}P(\eta_i,\eta_s)P_0(\eta_s,\eta_j)\,d\eta_s&=(1/2)\int_{-\infty}^{\infty}[P_0(\eta_i,\eta_s)P_0(\eta_s,\eta_j)+P_0(\eta_i,-\eta_s)P_0(-\eta_s,\eta_j)]\,d\eta_s\\&=(1/2)\left[\int_0^{\infty}P_0(\eta_i,\eta_s)P_0(\eta_s,\eta_j)\,d\eta_s+\int_{\infty}^{0}P_0(\eta_i,\eta_s)P_0(\eta_s,\eta_j)\,d\eta_s\right]\\&=(1/2)\int_{-\infty}^{\infty}P_0(\eta_i,\eta_s)P_0(\eta_s,\eta_j)\,d\eta_s.\end{aligned}\tag{A5}$$

Substituting (3.11a) into (A5) gives

$$\begin{aligned}\int_0^{\infty}P_0(\eta_i,\eta_s)P_0(\eta_s,\eta_j)\,d\eta_s&=(1/2)\int_{-\infty}^{\infty}[P(\eta_i-\eta_s)-P(\eta_i+\eta_s)][P(\eta_s-\eta_j)-P(\eta_s+\eta_j)]\,d\eta_s\\&=(1/2)[G(\eta_i-\eta_j)-G(\eta_i+\eta_j)-G(\eta_i+\eta_j)+G(\eta_i-\eta_j)]=G_0(\eta_i,\eta_j),\end{aligned}\tag{A6}$$

where (A1)–(A4) are used in the second last step. The result of (A6) gives (3.10a).

## APPENDIX B

### Derivation of (4.10)

Substituting (4.11) into the integral on the right-hand side of (4.10) gives

$$\begin{aligned}&\int_{-\pi}^{\pi}P_c(\beta_i-\beta_s)P_c(\beta_s-\beta_j)\,d\beta_s\\&=(\pi\Phi_i\Phi_j/2)^{-1/2}\textstyle\sum_n\sum_{n'}\int_{-\pi}^{\pi}d\beta_s\exp[-(\beta_i-\beta_s-2n\pi)^2/\Phi_i^2-(\beta_s-\beta_j-2n'\pi)^2/\Phi_j^2]\\&=(\pi\Phi_i\Phi_j/2)^{-1/2}\textstyle\sum_n\sum_{n'}\int_{n'}d\beta'\exp[-(\beta_{ij}-2n\pi-2n'\pi-\beta')^2/\Phi_i^2-\beta'^2/\Phi_j^2]\\&=(\pi\Phi_i\Phi_j/2)^{-1/2}\textstyle\sum_{n''}\sum_{n'}\int_{n'}d\beta'\exp[-(\beta_{ij}-2n''\pi)^2/\Phi_i^2+2(\beta_{ij}-2n''\pi)\beta'/\Phi_i^2-a^2\beta'^2]\\&=(\pi\Phi_i\Phi_j/2)^{-1/2}\textstyle\sum_{n''}\exp[-(\beta_{ij}-2n''\pi)^2(\Phi_i^{-2}-a^{-2}\Phi_i^{-4})]\sum_{n'}\int_{n'}d\beta'\exp\{-a^2[\beta'-(\beta_{ij}-2n''\pi)/(a\Phi_i)^2]^2\}\\&=(\pi\Phi_i\Phi_j/2)^{-1/2}\textstyle\sum_{n''}\exp[-(\beta_{ij}-2n''\pi)^2/(\Phi_i^2+\Phi_j^2)]\int_{-\infty}^{\infty}d\beta'\exp\{-a^2[\beta'-(\beta_{ij}-2n''\pi)/(a\Phi_i)^2]^2\}\\&=(\pi\Phi_i\Phi_j/2)^{-1/2}\textstyle\sum_{n''}\exp[-(\beta_{ij}-2n''\pi)^2/(\Phi_i^2+\Phi_j^2)]\int_{-\infty}^{\infty}d\beta'\exp(-a^2\beta''^2)\\&=[2\Phi_i\Phi_j/(\Phi_i^2+\Phi_j^2)]^{1/2}\textstyle\sum_{n''}\exp[-(\beta_i-\beta_j-2n''\pi)^2/(\Phi_i^2+\Phi_j^2)],\end{aligned}\tag{B1}$$

where $\beta_{ij}=\beta_i-\beta_j, n''=n+n', \beta'=\beta_s-\beta_j-2n'\pi, \int_{n'}d\beta'(\,)$ denotes the integration of $(\,)$ over $\beta'$ from $\beta'=-\pi-\beta_j-2n'\pi$ to $\beta'=\pi-\beta_j-2n'\pi$, $a^2=\Phi_i^{-2}+\Phi_j^{-2}$, and $\beta''=\beta'-(\beta_{ij}-2n''\pi)/(a\Phi_i)^2$.

The following transformations are used in the derivation of (B1): (i) The integration variable is transformed from $\beta_s$ to $\beta'=\beta_s-\beta_j-2n'\pi$ for each given integer value of $n'$ and thus

the integration range is changed from $(-\pi, \pi)$ to $(-\pi - \beta_j - 2n'\pi, \pi - \beta_j - 2n'\pi)$ as shown by the integral $\int_{n'} d\beta'(\ )$ in the second step of the derivation of (B1). (ii) The summation over integer $n$ from 0 to $\pm\infty$, denoted by $\sum_n$, is rearranged into the summation over $n''$ from 0 to $\pm\infty$, denoted by $\sum_{n''}$, in the third step. (iii) Once $n''$ is used in place of $n$, $n''$ is treated as a new index independent of $n'$, and this treatment is used in the fourth step. (iv) The integrand of $\int_{n'} d\beta'(\ )$ is invariant with respect to $n'$ (because its contained $n''$ is independent of $n'$), so $\sum_{n'}\int_{n'} d\beta'(\ ) = (\sum_{n'}\int_{n'}) d\beta'(\ ) = \int_{-\infty}^{\infty} d\beta'(\ )$, and this equality is used with $\Phi_i^{-2} - a^2\Phi_i^{-4} = \Phi_i^{-2}[1 - \Phi_j^2/(\Phi_i^2 + \Phi_j^2)] = 1/(\Phi_i^2 + \Phi_j^2)$ in the fifth step. (v) The integration variable is further transformed from $\beta'$ to $\beta'' = \beta' - (\beta_{ij} - 2n''\pi)/(a\Phi_i)^2$ in the second last step; (vi) $\int_{-\infty}^{\infty} d\beta'' \exp(-a^2\beta''^2) = \sqrt{\pi}/a = \sqrt{\pi}\Phi_i\Phi_j/(\Phi_i^2 + \Phi_j^2)^{1/2}$ is used in the last step of the derivation of (B1). Rewriting $n''$ into $n$, the result in the last step of (B1) gives $C(\beta_i - \beta_j)$ defined in (4.9), that is, the left-hand side of (4.10).

## APPENDIX C

### Derivation of (4.17)

Substituting $P_{3is}$ and $P_{4is}$ defined in (4.13) into (4.16) and then into (4.5) gives

$$V_R^a(r_i, h_i, \beta_i) = \sigma_3 \sum_{0s} X_{1is} c_{3s} - \sigma_4 \sum_s Y_{1is} c_{4s}, \tag{C1}$$

$$V_T^a(r_i, h_i, \beta_i) = \sigma_3 \sum_{0s} X_{2is} c_{3s} + \sigma_4 \sum_s Y_{2is} c_{4s}, \tag{C2}$$

$$w^a(r_i, h_i, \beta_i) = -\sigma_3 \sum_{0s} X_{3is} c_{3s}, \tag{C3}$$

where

$$\begin{aligned} X_{1is} = {} & \Big[F_i P_0'(r_i, r_s) P_c(\beta_i - \beta_s) dr/dR_i + F_i' P_0(r_i, r_s) P_c(\beta_i - \beta_s) \\ & + F_i P_0(r_i, r_s) \partial_{R_i} P_c(\beta_i - \beta_s)\Big][P_0'(h_i, h_s)/H \\ & + P_0(h_i, h_s)(d_z \ln\rho_a)_i](\Delta r \Delta h \Delta\beta)^{1/2}, \end{aligned} \tag{C4}$$

$$\begin{aligned} X_{2is} = {} & F_i P_0(r_i, r_s) P_c'(\beta_i - \beta_s)[P_0(h_i, h_s)/H \\ & + P_0(h_i, h_s)(d_z \ln\rho_a)_i](\Delta r \Delta h \Delta\beta)^{1/2}/R_i, \end{aligned} \tag{C5}$$

$$Y_{1is} = F_i P_0(r_i, r_s) P_c'(\beta_i - \beta_s) P(h_i - h_s)(\Delta r \Delta h \Delta\beta)^{1/2}/R_i, \tag{C6}$$

$$\begin{aligned} Y_{2is} = {} & \Big[F_i P_0'(r_i, r_s) P_c(\beta_i - \beta_s) dr/dR_i + F_i' P_0(r_i, r_s) P_c(\beta_i - \beta_s) \\ & + F_i P_0(r_i, r_s) \partial_{R_i} P_c(\beta_i - \beta_s)\Big] P(h_i - h_s)(\Delta r \Delta h \Delta\beta)^{1/2}, \end{aligned} \tag{C7}$$

$$\begin{aligned} X_{3is} = {} & \{R_i^{-1}[F_i P_0'(r_i, r_s) dr/dR_i + F_i' P_0(r_i, r_s)] P_c(\beta_i - \beta_s) + R_i^{-1} F_i P_0(r_i, r_s) \partial_R P_c(\beta_i - \beta_s) \\ & + F_i P_c(\beta_i - \beta_s)[P_0''(r_i, r_s)(dr/dR_i)^2 + P_0'(r_i, r_s) d^2r/dR_i^2] \\ & + F_i\Big[P_0(r_i, r_s)\partial_{R_i}^2 P_c(\beta_i - \beta_s) + 2\partial_{R_i} P_c(\beta_i - \beta_s) P_0'(r_i, r_s) dr/dR_i\Big] \\ & + 2F_i'\Big[P_0'(r_i, r_s) P_c(\beta_i - \beta_s) dr/dR_i + P_0(r_i, r_s)\partial_{R_i} P_c(\beta_i - \beta_s)\Big] \\ & + F_i'' P_0(r_i, r_s) P_c(\beta_i - \beta_s) + R_i^{-2} F_i P_0(r_i, r_s) P_c''(\beta_i - \beta_s)\} P_0(h_i, h_s)(\Delta r \Delta h \Delta\beta)^{1/2}. \end{aligned} \tag{C8}$$

Here, $P_0'(r_i, r_s)$, $P_0'(h_i, h_s)$, $dr/dR_i$, and $(d_z \ln\rho_a)_i$ are the same as those defined for $U_{is}$ and $W_{is}$ in (3.18), $d^2r/dR_i^2 = -R_i/[l(R_c^2 + R_i^2)^{3/2}]$, and

$$F_i \equiv F(R_i) = [\tanh(R_i/R_e)]^2,$$

$$F_i' \equiv dF_i/dR_i = 2\tanh(R_i/R_e)[\cosh(R_i/R_e)]^{-2}/R_e,$$

$$F_i'' \equiv d^2F_i/dR_i^2 = 2\{1 - 2[\sinh(R_i/R_e)]^2\}[\cosh(R_i/R_e)]^{-4}/R_e^2,$$

$$\begin{aligned} P_0''(r_i, r_s) &\equiv \partial^2 P_0(r_i, r_s)/\partial r_i^2 \\ &= 2(2/\pi)^{1/4}\{[1 - 2(r_i + r_s)^2]\exp[-(r_i + r_s)^2] - [1 - 2(r_i - r_s)^2]\exp[-(r_i - r_s)^2]\}, \end{aligned}$$

$$P_c'(\beta_i - \beta_s) \equiv \partial P_c(\beta_i - \beta_s)/\partial\beta_i = -2(2/\pi)^{1/4}\Phi_i^{-5/2}\sum_n(\beta_i - \beta_s - 2n\pi)\exp[-(\beta_i - \beta_s - 2n\pi)^2/\Phi_i^2],$$

$$\begin{aligned} P_c''(\beta_i - \beta_s) &\equiv \partial^2 P_c(\beta_i - \beta_s)/\partial\beta_i^2 \\ &= -2(2/\pi)^{1/4}\Phi_i^{-5/2}\sum_n[1 - 2(\beta_i - \beta_s - 2n\pi)^2/\Phi_i^2]\exp[-(\beta_i - \beta_s - 2n\pi)^2/\Phi_i^2], \end{aligned}$$

$$\begin{aligned} \partial_{R_i} P_c(\beta_i - \beta_s) &\equiv \partial P_c(\beta_i - \beta_s)/\partial R_i = \Phi_i'\partial P_c(\beta_i - \beta_s)/\partial\Phi_i \\ &= (2/\pi)^{1/4}\Phi_i'\sum_n[2(\beta_i - \beta_s - 2n\pi)^2\Phi_i^{-7/2} - \Phi_i^{-3/2}/2]\exp[-(\beta_i - \beta_s - 2n\pi)^2/\Phi_i^2] \end{aligned}$$

$$\partial_{R_i}^2 P_c(\beta_i - \beta_s) \equiv \partial^2 P_c(\beta_i - \beta_s)/\partial R_i^2 = \Phi_i''\,\partial P_c(\beta_i - \beta_s)/\partial\Phi_i + \Phi_i'^2\partial^2 P_c(\beta_i - \beta_s)/\partial\Phi_i^2$$

$$= (2/\pi)^{1/4}\{\Phi_i''\Phi_i^{-3/2}\sum_n[2(\beta_i-\beta_s-2n\pi)^2/\Phi_i^2-1/2]$$
$$+\Phi_i'^2\Phi_i^{-5/2}\sum_n[4(\beta_i-\beta_s-2n\pi)^4/\Phi_i^4-8(\beta_i-\beta_s-2n\pi)^2/\Phi_i^2+3/4]\}\exp[-(\beta_i-\beta_s-2n\pi)^2/\Phi_i^2],$$
$$\Phi_i' \equiv d\Phi_i/dR_i = [2\sinh(l/2)-\pi]R_p/(R_i+R_p)^2,$$
$$\Phi_i'' \equiv d^2\Phi_i/dR_i^2 = 2[\pi-2\sinh(l/2)]R_p/(R_i+R_p)^3.$$

Substituting (C1)–(C3) into (4.6) gives (4.17).

The divergence and vorticity computed from $\mathbf{u}^a$ are denoted and defined by $\delta^a \equiv \nabla'^2\chi$ and $\zeta^a \equiv \nabla'^2\psi$, respectively. Substituting (4.4) and (4.16) into these definitions gives

$$\delta^a(r_i,h_i,\beta_i) = \sigma_3\sum_{0s}X_{4is}c_{3s}, \tag{C9}$$
$$\zeta^a(r_i,h_i,\beta_i) = \sigma_4\sum_s Y_{4is}c_{4s}, \tag{C10}$$

where

$$X_{4is} = \{R_i^{-1}[F_iP_0'(r_i,r_s)dr/dR_i + F_i'P_0(r_i,r_s)]P_c(\beta_i-\beta_s) + R_i^{-1}F_iP_0(r_i,r_s)\partial_R P_c(\beta_i-\beta_s)$$
$$+ F_iP_c(\beta_i-\beta_s)[P_0''(r_i,r_s)(dr/dR_i)^2 + P_0'(r_i,r_s)d^2r/dR_i^2]$$
$$+ F_i\left[P_0(r_i,r_s)\partial_{R_i}^2P_c(\beta_i-\beta_s) + 2\partial_{R_i}P_c(\beta_i-\beta_s)P_0'(r_i,r_s)dr/dR_i\right]$$
$$+ 2F_i'\left[P_0'(r_i,r_s)P_c(\beta_i-\beta_s)dr/dR_i + P_0(r_i,r_s)\partial_{R_i}P_c(\beta_i-\beta_s)\right]$$
$$+ F_i''P_0(r_i,r_s)P_c(\beta_i-\beta_s) + R_i^{-2}F_iP_0(r_i,r_s)P_c''(\beta_i-\beta_s)\}[P_0'(h_i,h_s) + P_0(h_i,h_s)(d_z\ln\rho_a)_i],$$
$$Y_{4is} = \{R_i^{-1}[F_iP_0'(r_i,r_s)dr/dR_i + F_i'P_0(r_i,r_s)]P_c(\beta_i-\beta_s) + R_i^{-1}F_iP_0(r_i,r_s)\partial_R P_c(\beta_i-\beta_s)$$
$$+ F_iP_c(\beta_i-\beta_s)[P_0''(r_i,r_s)(dr/dR_i)^2 + P_0'(r_i,r_s)d^2r/dR_i^2]$$
$$+ F_i\left[P_0(r_i,r_s)\partial_{R_i}^2P_c(\beta_i-\beta_s) + 2\partial_{R_i}P_c(\beta_i-\beta_s)P_0'(r_i,r_s)dr/dR_i\right]$$
$$+ 2F_i'\left[P_0'(r_i,r_s)P_c(\beta_i-\beta_s)dr/dR_i + P_0(r_i,r_s)\partial_{R_i}P_c(\beta_i-\beta_s)\right]$$
$$+ F_i''P_0(r_i,r_s)P_c(\beta_i-\beta_s) + R_i^{-2}F_iP_0(r_i,r_s)P_c''(\beta_i-\beta_s)\}P(h_i-h_s).$$

Note that $R_i \to 0$ as $r_i \to 0$, $F_i \to O(R_i^2) \to 0$ and $F_i' \to O(R_i) \to 0$ as $R_i \to 0$, $P_0(r_i, r_s) \to 0$ and $P_0''(r_i, r_s) \to 0$ as $r_i \to 0$, and $P_0(h_i, h_s) \to 0$ as $h_i \to 0$. Applying these properties to (C4)–(C10), it is easy to see that the matrix element terms $X_{1is}$, $X_{2is}$, $X_{3is}$, $X_{4is}$, $Y_{1is}$, $Y_{2is}$, and $Y_{4is}$ all approach zero as $R_i \to 0$, and $X_{3is}$ approaches zero as $h_i \to 0$. Substituting these results into (C1)–(C3) and (C9)–(C10) gives $V_R^a \to 0$, $V_T^a \to 0$, $w^a \to 0$, $\delta^a \to 0$, and $\zeta^a \to 0$ as $R_i \to 0$, and $w^a \to 0$ as $h_i \to 0$. Thus, the required boundary conditions (stated the end of section 2c) are satisfied automatically. In addition, $\delta^a$ and $\zeta^a$ also approach zero as $R_i \to 0$, and these additional conditions are necessary for the convergence of $\delta^a$ and $\zeta^a$ in the limit of $R_i \to 0$. The convergence of $w^a$, $\delta^a$, and $\zeta^a$ in the limit of $R_i \to 0$ requires both $F_i$ and $F_i' \to 0$ as $R_i \to 0$. For example, if $F$ is defined by $\tanh(R/R_e)$ instead of $[\tanh(R/R_e)]^2$, then $F \to 0$ but $F' = [\cosh(R/R_e)]^{-2}/R_e \to 1/R_e \neq 0$ as $R \to 0$. In this case, it is easy to see from (C3) [or (C9), (C10)] that $w^a$ (or $\delta^a$, $\zeta^a$) is not ensured to converge to a single value (which is zero for a purely asymmetric field) at $R = 0$ because it can approach different values as $R \to 0$ from different azimuthal directions (with $\beta$ fixed to different values), although $V_R^a$ and $V_T^a$ still approach zero as $R \to 0$. Furthermore, if $F$ is simply set to 1, then $w^a$, $\delta^a$, and $\zeta^a$ become singular at $R = 0$ while $V_R^a$ in (C1) and $V_T^a$ in (C2) are not ensured to converge to a single value at $R = 0$. The above analyses explain why $F \equiv [\tanh(R/R_e)]^2$ is introduced to modulate the background error standard deviations of $X$ and $Y$ (mainly in the vortex core), as shown in (4.8) where $F$ is combined into $\gamma \equiv \rho_a F$.

## REFERENCES


Bluestein, H. B., K. J. Thiem, J. C. Snyder, and J. B. Houser, 2019: Tornadogenesis and early tornado evolution in the El Reno, Oklahoma, supercell on 31 May 2013. *Mon. Wea. Rev.*, **147**, 2045–2066, https://doi.org/10.1175/MWR-D-18-0338.1.

Caillault, K., and Y. Lemaitre, 1999: Retrieval of three-dimensional wind fields corrected for the time-induced advection problem. *J. Atmos. Oceanic Technol.*, **16**, 708–722, https://doi.org/10.1175/1520-0426(1999)016<0708:ROTDWF>2.0.CO;2.

Chong, M., J. Testud, and F. Roux, 1983: Three-dimensional wind field analysis from dual-Doppler radar data. Part II: Minimizing the error due to temporal variation. *J. Climate Appl. Meteor.*, **22**, 1216–1226, https://doi.org/10.1175/1520-0450(1983)022<1216:TDWFAF>2.0.CO;2.

Gal-Chen, T., 1982: Errors in fixed and moving frame of references: Applications for conventional and Doppler radar analysis. *J. Atmos. Sci.*, **39**, 2279–2300, https://doi.org/10.1175/1520-0469(1982)039<2279:EIFAMF>2.0.CO;2.

Gao, J., and D. Stensrud, 2014: Some observing system simulation experiments with a hybrid 3DEnVAR system for storm-scale radar DA. *Mon. Wea. Rev.*, **142**, 3326–3346, https://doi.org/10.1175/MWR-D-14-00025.1.

——, and Coauthors, 2013: A real-time weather-adaptive 3DVAR analysis system for severe weather detections and warnings. *Wea. Forecasting*, **28**, 727–745, https://doi.org/10.1175/WAF-D-12-00093.1.

Jones, T. A., and Coauthors, 2016: Storm-scale DA and ensemble forecasting with the NSSL experimental Warn-on-Forecast System. Part II: Combined radar and satellite data

experiments. *Wea. Forecasting*, **31**, 297–327, https://doi.org/10.1175/WAF-D-15-0107.1.

Kurdzo, J. M., and Coauthors, 2017: Observations of severe local storms and tornadoes with the Atmospheric Imaging Radar. *Bull. Amer. Meteor. Soc.*, **98**, 915–935, https://doi.org/10.1175/BAMS-D-15-00266.1.

Lee, W. C., and J. Wurman, 2005: Diagnosed three-dimensional axisymmetric structure of the Mulhall tornado on 3 May 1999. *J. Atmos. Sci.*, **62**, 2373–2393, https://doi.org/10.1175/JAS3489.1.

Liou, Y., 1999: Single radar recovery of cross-beam wind components using a modified moving frame of reference technique. *J. Atmos. Oceanic Technol.*, **16**, 1003–1016, https://doi.org/10.1175/1520-0426(1999)016<1003:SRROCB>2.0.CO;2.

——, 2002: An explanation of the wind speed underestimation obtained from a least squares type of single-Doppler radar velocity retrieval method. *J. Appl. Meteor.*, **41**, 811–823, https://doi.org/10.1175/1520-0450(2002)041<0811:AEOTWS>2.0.CO;2.

——, H. B. Bluestein, M. M. French, and Z. B. Wienhoff, 2018: Single-Doppler velocity retrieval of the wind field in a tornadic supercell using mobile, phased-array, Doppler radar data. *J. Atmos. Oceanic Technol.*, **35**, 1649–1663, https://doi.org/10.1175/JTECH-D-18-0004.1.

Liu, S., C. Qiu, Q. Xu, and P. Zhang, 2004: An improved time interpolation for three-dimensional Doppler wind analysis. *J. Appl. Meteor.*, **43**, 1379–1391, https://doi.org/10.1175/JAM2150.1.

——, M. Xue, and Q. Xu, 2007: Using wavelet analysis to detect tornadoes from Doppler radar radial-velocity observations. *J. Atmos. Oceanic Technol.*, **24**, 344–359, https://doi.org/10.1175/JTECH1989.1.

Newman, J. F., V. Lakshmanan, P. L. Heinselman, M. B. Richman, and T. M. Smith, 2013: Range-correcting azimuthal shear in Doppler radar data. *Wea. Forecasting*, **28**, 194–211, https://doi.org/10.1175/WAF-D-11-00154.1.

NOAA, 2014: Strategic plan for NOAA's Office of Oceanic and Atmospheric Research. NOAA Rep., 29 pp., https://research.noaa.gov/sites/oar/Documents/OARStrategicPlan.pdf.

Potvin, C. K., A. Shapiro, T. Y. Yu, J. Gao, and M. Xue, 2009: Using a low-order model to detect and characterize tornadoes in multiple-Doppler radar data. *Mon. Wea. Rev.*, **137**, 1230–1249, https://doi.org/10.1175/2008MWR2446.1.

——, ——, M. I. Biggerstaff, and J. M. Wurman, 2011: The VDAC technique: A variational method for detecting and characterizing convective vortices in multiple-Doppler radar data. *Mon. Wea. Rev.*, **139**, 2593–2613, https://doi.org/10.1175/2011MWR3638.1.

Shapiro, A., K. M. Willingham, and C. K. Potvin, 2010: Spatially variable advection correction of radar data. Part I: Theoretical considerations. *J. Atmos. Sci.*, **67**, 3445–3456, https://doi.org/10.1175/2010JAS3465.1.

——, S. Rahimi, C. K. Potvin, and L. Orf, 2015: On the use of advection correction in trajectory calculations. *J. Atmos. Sci.*, **72**, 4261–4280, https://doi.org/10.1175/JAS-D-15-0095.1.

Skinner, P. S., and Coauthors, 2018: Object-based verification of a prototype warn-on-forecast system. *Wea. Forecasting*, **33**, 1225–1250, https://doi.org/10.1175/WAF-D-18-0020.1.

Snook, N., Y. Jung, J. Brotzge, B. Putnam, and M. Xue, 2016: Prediction and ensemble forecast verification of hail in the supercell storms of 20 May 2013. *Wea. Forecasting*, **31**, 811–825, https://doi.org/10.1175/WAF-D-15-0152.1.

——, M. Xue, and Y. Jung, 2019: Tornado-resolving ensemble and probabilistic predictions of the 20 May 2013 Newcastle–Moore EF5 tornado. *Mon. Wea. Rev.*, **147**, 1215–1235, https://doi.org/10.1175/MWR-D-18-0236.1.

Stensrud, D. J., and Coauthors, 2009: Convective-scale warn on forecast: A vision for 2020. *Bull. Amer. Meteor. Soc.*, **90**, 1487–1499, https://doi.org/10.1175/2009BAMS2795.1.

——, and Coauthors, 2013: Progress and challenges with warn-on-forecast. *Atmos. Res.*, **123**, 2–16, https://doi.org/10.1016/j.atmosres.2012.04.004.

Stumpf, G. J., and Coauthors, 1998: The National Severe Storms Laboratory mesocyclone detection algorithm for the WSR-88D. *Wea. Forecasting*, **13**, 304–326, https://doi.org/10.1175/1520-0434(1998)013<0304:TNSSLM>2.0.CO;2.

Wang, Y., and Coauthors, 2019: Test of a weather-adaptive dual-resolution hybrid warn-on-forecast analysis and forecast system for several severe weather events. *Wea. Forecasting*, **34**, 1807–1827, https://doi.org/10.1175/WAF-D-19-0071.1.

Wheatley, D. M., K. H. Knopfmeier, T. A. Jones, and G. J. Creager, 2015: Storm-scale DA and ensemble forecasting with the NSSL Experimental Warn-on-Forecast System. Part I: Radar data experiments. *Wea. Forecasting*, **30**, 1795–1817, https://doi.org/10.1175/WAF-D-15-0043.1.

Wood, V. T., and R. A. Brown, 1997: Effects of radar sampling on single-Doppler velocity signatures of mesocyclones and tornadoes. *Wea. Forecasting*, **12**, 928–938, https://doi.org/10.1175/1520-0434(1997)012<0928:EORSOS>2.0.CO;2.

——, and ——, 2011: Simulated tornadic vortex signatures of tornado-like vortices having one- and two-celled structures. *J. Appl. Meteor. Climatol.*, **50**, 2338–2342, https://doi.org/10.1175/JAMC-D-11-0118.1.

Wurman, J., and K. Kosiba, 2018: The role of small-scale vortices in enhancing surface winds and damage in Hurricane Harvey (2017). *Mon. Wea. Rev.*, **146**, 713–722, https://doi.org/10.1175/MWR-D-17-0327.1.

Xu, Q., 2019: On the choice of momentum control variables and covariance modeling for mesoscale data assimilation. *J. Atmos. Sci.*, **76**, 89–111, https://doi.org/10.1175/JAS-D-18-0093.1.

——, and L. Wei, 2020: A variational method for analyzing vortex flows in radar-scanned tornadic mesocyclones. Part II: Tests with analytically formulated vortices. *J. Atmos. Sci.*, **78**, 843–861, https://doi.org/10.1175/JAS-D-20-0159.1.

——, K. Nai, and L. Wei, 2007a: An innovation method for estimating radar radial-velocity observation error and background wind error covariances. *Quart. J. Roy. Meteor. Soc.*, **133**, 407–415, https://doi.org/10.1002/qj.21.

——, ——, ——, H. Lu, P. Zhang, S. Liu, and D. Parrish, 2007b: Estimating radar wind observation error and NCEP WRF background wind error covariances from radar radial-velocity innovations. *18th Conf. on Numerical Weather Prediction*, Park City, UT, Amer. Meteor. Soc., 1B.3, https://ams.confex.com/ams/22WAF18NWP/techprogram/paper_123419.htm.

——, L. Wei, W. Gu, J. Gong, and Q. Zhao, 2010: A 3.5-dimensional variational method for Doppler radar data assimilation and its application to phased-array radar observations. *Adv. Meteor.*, **2010**, 797265, https://doi.org/10.1155/2010/797265.

——, ——, K. Nai, S. Liu, R. M. Rabin, and Q. Zhao, 2015a: A radar wind analysis system for nowcast applications. *Adv. Meteor.*, **2015**, 264515, https://doi.org/10.1155/2015/264515.

——, ——, and ——, 2015b: Analyzing vortex winds in radar-observed tornadic mesocyclones for nowcast applications. *Wea. Forecasting*, **30**, 1140–1157, https://doi.org/10.1175/WAF-D-15-0046.1.

——, ——, J. Gao, and Q. Zhao, K. Nai and S. Liu, 2016: Multistep variational data assimilation: Important issues and a spectral approach. *Tellus*, **68A**, 31110, https://doi.org/10.3402/tellusa.v68.31110.

——, ——, and K. Nai, 2017: A three-step method for estimating vortex center locations in four-dimensional space from radar-observed tornadic mesocyclones. *J. Atmos. Oceanic Technol.*, **34**, 2275–2281, https://doi.org/10.1175/JTECH-D-17-0123.1.

Yang, S., and Q. Xu, 1996: Statistical errors in variational data assimilation—A theoretical one-dimensional analysis applied to Doppler wind retrieval. *J. Atmos. Sci.*, **53**, 2563–2577, https://doi.org/10.1175/1 520-0469(1996)053<2563:SEIVDA>2.0.CO;2.

Zhang, J., and T. Gal-Chen, 1996: Single-Doppler wind retrieval in the moving frame of reference. *J. Atmos. Sci.*, **53**, 2609–2623, https://doi.org/10.1175/1520-0469(1996)053<2609:SDWRIT>2.0.CO;2.